# Calculation of Axisymmetric Stability in an Inverse Aspect-Ratio Expanded Tokamak Plasma Equilibrium

Richard Fitzpatrick [a]

*Institute for Fusion Studies, Department of Physics,*

*University of Texas at Austin, Austin, TX 78712*

The stability of axisymmetric modes in an aspect-ratio expanded tokamak plasma equilibrium surrounded by a conformal resistive wall is calculated. The calculation turns out to be significantly different to the calculation of the stability of non-axisymmetric ideal modes in an aspect-ratio expanded equilibrium. In particular, the role of the toroidal angular momentum flux (which is identically zero for an axisymmetric mode) is instead played by the electromagnetic energy flux. The conservation of electromagnetic energy is used to prove that the perturbed plasma potential energy matrix is Hermitian. Positive triangularity is found to have a stabilizing effect on the vertical mode in vertically elongated plasmas, whereas negative triangularity has a marked destabilizing effect. Lack of up-down symmetry is found to have a destabilizing effect on the vertical mode. It is concluded that finite wall thickness should be taken into account when calculating the maximum controllable plasma elongation of a tokamak plasma.

[a] rfitzp@utexas.edu

## I. INTRODUCTION

It is well known that an increase in the net toroidal plasma current flowing around a tokamak leads to an enhancement of both the maximum stable $\beta$ value and the energy confinement time.[1,2] The conventional method of maximizing the total plasma current, without degrading the stability of the system to non-axisymmetric magnetohydrodynamical (MHD) modes, is to modify the plasma's poloidal cross-section such that it is both vertically elongated and triangular.[3] Unfortunately, tokamak plasmas possessing strong cross-sectional shaping are subject to severe axisymmetric instabilities.[4,5] Such instabilities involve bulk vertical motion of the plasma on an Alfvénic timescale (i.e., $10^{-7}$ s), which results in the sudden and violent termination of the discharge when it comes into contact with the first wall. It is possible to stabilize an axisymmetric mode by placing a perfectly conducting wall around the plasma. In reality, the mode remains unstable because the wall inevitably possesses finite electrical conductivity.[6] However, growth time of the mode is increased from the Alfvén time to the very much longer characteristic L/R time of the wall.[7–9] Usually, the vacuum vessel plays the role of the wall, and has an L/R time that is well in excess of $10^{-3}$ s. Such a time is much shorter than the length of the plasma discharge, but is still long enough to allow active feedback stabilization of the axisymmetric mode with practical power supplies.[10]

Ref. 11 describes the TJ toroidal tearing mode code, which calculates the stability of an inverse aspect-ratio expanded tokamak plasma equilibrium to *non-axisymmetric* tearing modes via asymptotic matching techniques. Ref. 12 describes a generalization of the TJ code that permits it to calculate the stability of the plasma to non-axisymmetric ideal modes in the presence of a perfectly conducting wall surrounding the plasma. The aim of this paper is to describe a further generalization the TJ code that allows it to calculate the stability of the plasma to *axisymmetric* ideal modes in the presence of a resistive wall that surrounds the plasma. It might be hope that, in order to investigate axisymmetric modes, we could simply take the existing TJ code and set the toroidal mode number, $n$, to zero. Unfortunately, this simple scheme does not work, as evidenced by the large number of terms involving $n^{-1}$ in the analysis of Ref. 11. Hence, as described in this paper, it is necessary to redo much of the

TJ analysis for the special case $n = 0$.

The simplified approach to calculating the vertical stability of tokamak plasmas described in this paper is quite different to that described in Refs. 13 and 14. In fact, Refs. 13 and 14 employ up-down symmetric, analytic Solov'ev plasma equilibria in which the equilibrium current jumps discontinuously to zero across the plasma-vacuum interface. Such equilibria can have arbitrary aspect-ratios, and possess the simplifying property that the perturbed plasma currents generated by vertical instabilities are surface currents that are localized on the interface. On the other hand, this paper employs realistic diffuse plasma equilibria in which the equilibrium current goes smoothly to zero as the plasma-vacuum interface is crossed, and in which the perturbed plasma currents associated with vertical instabilities are distributed throughout the plasma volume. In addition, our equilibria can be non up-down symmetric. Our main simplifying approximation is to restrict the inverse aspect-ratio of the plasma to only take small values.

This paper is organized as follows. In Sect. II, we introduce a general axisymmetric plasma equilibrium. In Sect. III, we examine axisymmetric perturbations to this equilibrium. Magnetic perturbations in the vacuum region surrounding the plasma are discussed in Sect. IV. The stability of the equilibrium to ideal axisymmetric modes is examined in Sect. V. The stability of the equilibrium to axisymmetric resistive wall modes is discussed in Sect. VI. The large aspect-ratio approximation is introduced in Sect. VII. The results of the calculations performed with the enhanced version of the TJ code are presented in Ref. VIII. Finally, the paper is summarized in Sect. IX.

## II. GENERAL PLASMA EQUILIBRIUM

All lengths in this paper are normalized to the major radius of the plasma magnetic axis, $R_0$. All magnetic field-strengths are normalized to the toroidal field-strength at the magnetic axis, $B_0$. All current densities are normalized to $B_0/(\mu_0\, R_0)$. All plasma pressures are normalized to $B_0^2/\mu_0$. All energies are normalized to $B_0^2\, R_0^3/\mu_0$.

Let $R$, $\phi$, $Z$ be right-handed cylindrical coordinates whose Jacobian is $(\nabla R\times\nabla\phi\cdot\nabla Z)^{-1} =$

$R$. Note that $|\nabla\phi| = 1/R$. Let $r$, $\theta$, $\phi$ be right-handed flux-coordinates whose Jacobian is [15,16]

$$\mathcal{J}(r,\theta) \equiv (\nabla r \times \nabla\theta \cdot \nabla\phi)^{-1} \equiv R\left(\frac{\partial R}{\partial\theta}\frac{\partial Z}{\partial r} - \frac{\partial R}{\partial r}\frac{\partial Z}{\partial\theta}\right) = r\,R^2. \tag{1}$$

Note that $r = r(R,Z)$ and $\theta = \theta(R,Z)$. The magnetic axis corresponds to $r = 0$. The plasma-vacuum interface corresponds to $r = a$. The inboard mid-plane corresponds to $\theta = 0$.

Consider an axisymmetric tokamak equilibrium whose magnetic field takes the form

$$\mathbf{B}(r,\theta) = f(r)\,\nabla\phi \times \nabla r + g(r)\,\nabla\phi = f\,\nabla(\phi - q\,\theta) \times \nabla r, \tag{2}$$

where

$$q(r) = \frac{r\,g}{f} \tag{3}$$

is the safety-factor profile. Note that $\mathbf{B}\cdot\nabla r = 0$, which implies that $r$ is a magnetic flux-surface label. We require $g = 1$ on the magnetic axis in order to ensure that the normalized toroidal magnetic field-strength at the axis is unity.

It is easily demonstrated that [11]

$$B^r = \mathbf{B}\cdot\nabla r = 0, \tag{4}$$

$$B^\theta = \mathbf{B}\cdot\nabla\theta = \frac{f}{r\,R^2}, \tag{5}$$

$$B^\phi = \mathbf{B}\cdot\nabla\phi = \frac{g}{R^2}, \tag{6}$$

$$B_r = \mathcal{J}\,\nabla\theta\times\nabla\phi\cdot\mathbf{B} = -r\,f\,\nabla r\cdot\nabla\theta, \tag{7}$$

$$B_\theta = \mathcal{J}\,\nabla\phi\times\nabla r\cdot\mathbf{B} = r\,f\,|\nabla r|^2, \tag{8}$$

$$B_\phi = \mathcal{J}\,\nabla r\times\nabla\theta\cdot\mathbf{B} = g. \tag{9}$$

The Maxwell equation (neglecting the displacement current, because the plasma velocity perturbations due to axisymmetric modes are far smaller than the velocity of light in vacuum) $\mathbf{J} = \nabla\times\mathbf{B}$ yields

$$\mathcal{J}\,J^r = \frac{\partial B_\phi}{\partial\theta} = 0, \tag{10}$$

$$\mathcal{J}\,J^\theta = -\frac{\partial B_\phi}{\partial r} = -g', \tag{11}$$

$$\mathcal{J}\, J^{\phi} = \frac{\partial B_\theta}{\partial r} - \frac{\partial B_r}{\partial \theta} = \frac{\partial}{\partial r}\big(r\, f\, |\nabla r|^2\big) + \frac{\partial}{\partial \theta}(r\, f\, \nabla r \cdot \nabla \theta)\,, \tag{12}$$

where $\mathbf{J}$ is the equilibrium current density, $' \equiv d/dr$, and use has been made of Eqs. (7)–(9).

Equilibrium force balance requires that

$$\nabla P = \mathbf{J} \times \mathbf{B}, \tag{13}$$

where $P(r)$ is the equilibrium scalar plasma pressure. Here, for the sake of simplicity, we have neglected the small centrifugal modifications to force balance due to subsonic plasma rotation.[17,18] It follows that

$$P' = \mathcal{J}(J^\theta\, B^\phi - J^\phi\, B^\theta) = -g'\, \frac{g}{R^2} - \frac{f}{r\, R^2}\left[\frac{\partial}{\partial r}\big(r\, f\, |\nabla r|^2\big) + \frac{\partial}{\partial \theta}(r\, f\, \nabla r \cdot \nabla \theta)\right], \tag{14}$$

where use has been made of Eqs. (4)–(6), and (10)–(12). The other two components of Eq. (13) are identically zero.

Equation (14) yields the *inverse Grad-Shafranov equation*:[16]

$$\frac{f}{r}\,\frac{\partial}{\partial r}\big(r\, f\, |\nabla r|^2\big) + \frac{f}{r}\,\frac{\partial}{\partial \theta}(r\, f\, \nabla r \cdot \nabla \theta) + g\, g' + R^2\, P' = 0. \tag{15}$$

It follows from Eqs. (3), (12), and (15) that

$$\mathcal{J}\, J^{\phi} = -q\, g' - \frac{r\, R^2\, P'}{f}. \tag{16}$$

It is clear from Eqs. (11) and (16) that $g' = P' = 0$ in the current-free "vacuum" region surrounding the plasma, $r \geq a$. We shall also assume that $g' = P' = 0$ at the plasma-vacuum interface, so as to ensure that the equilibrium plasma current density is zero at the interface, $r = a$.

## III. GENERAL AXISYMMETRIC PLASMA PERTURBATION

### A. Derivation of Axisymmetric Ideal-MHD P.D.E.s

Let us assume that all perturbed quantities have no dependence on the toroidal angle, $\phi$. The perturbed plasma equilibrium satisfies the linearized, marginally-stable, ideal-MHD equations [16,19,27]

$$\mathbf{b} = \nabla \times (\boldsymbol{\xi} \times \mathbf{B}), \tag{17}$$

$$\nabla p = \mathbf{j} \times \mathbf{B} + \mathbf{J} \times \mathbf{b}, \tag{18}$$

$$\mathbf{j} = \nabla \times \mathbf{b}, \tag{19}$$

$$p = -\boldsymbol{\xi} \cdot \nabla P, \tag{20}$$

where $\boldsymbol{\xi}(r,\theta)$ is the plasma displacement, $\mathbf{b}(r,\theta)$ the perturbed magnetic field, $\mathbf{j}(r,\theta)$ the perturbed current density, and $p(r,\theta)$ the perturbed scalar pressure.

Now,[11]

$$(\boldsymbol{\xi} \times \mathbf{B})_\theta = \mathcal{J}\,(\xi^\phi\, B^r - \xi^r\, B^\phi) = -\mathcal{J}\, B^\phi\, \xi^r, \tag{21}$$

$$(\boldsymbol{\xi} \times \mathbf{B})_\phi = \mathcal{J}\,(\xi^r\, B^\theta - \xi^\theta\, B^r) = \mathcal{J}\, B^\theta\, \xi^r, \tag{22}$$

where use has been made of the fact that $B^r = J^r = 0$. [See Eqs. (4) and (10).] Combining Eqs. (17) and (22), we obtain

$$\mathcal{J}\, b^r = \frac{\partial}{\partial \theta}\left(\mathcal{J}\, B^\theta\, \xi^r\right). \tag{23}$$

Thus, Eqs. (1), (3), and (5) give [11]

$$r\, R^2\, b^r = \frac{\partial y}{\partial \theta}, \tag{24}$$

where

$$y(r,\theta) = f\, \xi^r. \tag{25}$$

The constraint $\nabla \cdot \mathbf{b} = 0$, which follows from Eq. (17), immediately yields

$$r\, R^2\, b^\theta = -\frac{\partial y}{\partial r}. \tag{26}$$

Note that the preceding expression is radically different from the expression, (54), for $b^\theta$ given in Ref. 11. Thus, it is at this stage that our analysis starts to diverge from that of Ref. 11.

According to Eq. (20),

$$p = -P'\, \nabla r \cdot \boldsymbol{\xi} = -P'\, \xi^r. \tag{27}$$

So, the perturbed force balance equation, (18), yields

$$-\frac{\partial\,(P'\,\xi^r)}{\partial r} = (\mathbf{j}\times\mathbf{B})_r + (\mathbf{J}\times\mathbf{b})_r, \tag{28}$$

$$-\frac{\partial\,(P'\,\xi^r)}{\partial \theta} = (\mathbf{j}\times\mathbf{B})_\theta + (\mathbf{J}\times\mathbf{b})_\theta, \tag{29}$$

$$0 = (\mathbf{j}\times\mathbf{B})_\phi + (\mathbf{J}\times\mathbf{b})_\phi, \tag{30}$$

giving [11]

$$-\frac{\partial\,(P'\,\xi^r)}{\partial r} = r\,R^2\,(j^\theta\,B^\phi - j^\phi\,B^\theta) + r\,R^2\,(J^\theta\,b^\phi - J^\phi\,b^\theta), \tag{31}$$

$$-\frac{\partial\,(P'\,\xi^r)}{\partial \theta} = r\,R^2\,(j^\phi\,B^r - j^r\,B^\phi) + r\,R^2\,(J^\phi\,b^r - J^r\,b^\phi), \tag{32}$$

$$0 = r\,R^2\,(j^r\,B^\theta - j^\theta\,B^r) + r\,R^2\,(J^r\,b^\theta - J^\theta\,b^r), \tag{33}$$

where use has been made of Eq. (1). Thus, according to Eqs. (4)–(6), (10), (11), and (16),

$$-\frac{\partial\,(P'\,\xi^r)}{\partial r} = f\,(q\,j^\theta - j^\phi) - g'\,b^\phi + \left(q\,g' + \frac{r\,R^2\,P'}{f}\right) b^\theta, \tag{34}$$

$$-\frac{\partial\,(P'\,\xi^r)}{\partial \theta} = -r\,g\,j^r - \left(q\,g' + \frac{r\,R^2\,P'}{f}\right) b^r, \tag{35}$$

$$0 = f\,j^r + g'\,b^r. \tag{36}$$

It follows from Eqs. (24) and (36) that

$$r\,R^2\,j^r = -\alpha_g\,\frac{\partial y}{\partial \theta}, \tag{37}$$

where

$$\alpha_g(r) = \frac{g'}{f}. \tag{38}$$

Note that Eq. (35) is trivially satisfied. Hence, of the three components of the perturbed force balance equation, only Eq. (34) remains to be solved.

Equation (19) yields [11]

$$r\,R^2\,j^r = \frac{\partial b_\phi}{\partial \theta}, \tag{39}$$

$$r\,R^2\,j^\theta = -\frac{\partial b_\phi}{\partial r}, \tag{40}$$

$$r\,R^2\,j^{\,\phi} = \frac{\partial b_\theta}{\partial r} - \frac{\partial b_r}{\partial \theta}, \tag{41}$$

where use has been made of Eq. (1). It follows from Eqs. (37), (39), and (40) that

$$b_\phi = -\alpha_g\, y, \tag{42}$$

$$r\,R^2\,j^{\,\theta} = \frac{\partial(\alpha_g\, y)}{\partial r}. \tag{43}$$

Note that $\nabla\cdot\mathbf{j} = 0$, in accordance with Eq. (19).

Now,

$$\mathbf{b} = b_r\,\nabla r + b_\theta\,\nabla\theta + b_\phi\,\nabla\phi, \tag{44}$$

so

$$b^r = \mathbf{b}\cdot\nabla r = |\nabla r|^2\,b_r + (\nabla r\cdot\nabla\theta)\,b_\theta, \tag{45}$$

$$b^{\,\theta} = \mathbf{b}\cdot\nabla\theta = (\nabla r\cdot\nabla\theta)\,b_r + |\nabla\theta|^2\,b_\theta, \tag{46}$$

$$b^{\,\phi} = \mathbf{b}\cdot\nabla\phi = \frac{b_\phi}{R^2}. \tag{47}$$

Equations (1), (45), and (46) can be rearranged to give [11]

$$b_r = \left(\frac{1}{|\nabla r|^2}\right) b^r - \left(\frac{\nabla r\cdot\nabla\theta}{|\nabla r|^2}\right) b_\theta, \tag{48}$$

$$b^{\,\theta} = \left(\frac{\nabla r\cdot\nabla\theta}{|\nabla r|^2}\right) b^r + \left(\frac{1}{r^2\,R^2\,|\nabla r|^2}\right) b_\theta. \tag{49}$$

Let

$$\mathcal{Z}(r,\theta) = |\nabla r|^2\,r\,\frac{\partial y}{\partial r} + r\,\nabla r\cdot\nabla\theta\,\frac{\partial y}{\partial\theta}. \tag{50}$$

Equations (24), (26), (42), (48) and (49) yield

$$b_r = \frac{1}{r\,|\nabla r|^2\,R^2}\,\frac{\partial y}{\partial\theta} + \frac{\nabla r\cdot\nabla\theta}{|\nabla r|^2}\,\mathcal{Z}, \tag{51}$$

$$b_\theta = -\mathcal{Z}, \tag{52}$$

$$b^{\,\phi} = -\frac{\alpha_g}{R^2}\,y. \tag{53}$$

Equations (41), (51), and (52) give

$$r\,R^2\,j^{\,\phi} = -\frac{\partial\mathcal{Z}}{\partial r} - \frac{\partial}{\partial\theta}\left[\frac{1}{r\,|\nabla r|^2\,R^2}\,\frac{\partial y}{\partial\theta} + \frac{\nabla r\cdot\nabla\theta}{|\nabla r|^2}\,\mathcal{Z}\right]. \tag{54}$$

It follows from Eqs. (25), (26), (34), (43), (53), and (54) that

$$-\frac{\partial}{\partial r}\left(\frac{P'}{f}\,y\right) = \frac{f\,q}{r\,R^2}\,\frac{\partial(\alpha_g\,y)}{\partial r} + \frac{f}{r\,R^2}\,\frac{\partial \mathcal{Z}}{\partial r} + \frac{f}{r\,R^2}\,\frac{\partial}{\partial\theta}\left[\frac{1}{r\,|\nabla r|^2\,R^2}\,\frac{\partial y}{\partial\theta} + \frac{\nabla r\cdot\nabla\theta}{|\nabla r|^2}\,\mathcal{Z}\right] + \frac{g'\,\alpha_g}{R^2}\,y - \left(q\,g' + \frac{r\,R^2\,P'}{f}\right)\frac{1}{r\,R^2}\,\frac{\partial y}{\partial r}. \tag{55}$$

Hence,

$$-\left[(\alpha_f\,\alpha_p + r\,\alpha_p')R^2 + q\,r\,\alpha_g' + r^2\,\alpha_g^2\right]y = r\,\frac{\partial\mathcal{Z}}{\partial r} + \frac{\partial}{\partial\theta}\left[\frac{1}{|\nabla r|^2\,R^2}\,\frac{\partial y}{\partial\theta} + \frac{r\,\nabla r\cdot\nabla\theta}{|\nabla r|^2}\,\mathcal{Z}\right], \tag{56}$$

$$R^2\,j^{\,\phi} = \left[(\alpha_f\,\alpha_p + r\,\alpha_p')R^2 + q\,r\,\alpha_g' + r^2\,\alpha_g^2\right]y, \tag{57}$$

where

$$\alpha_p(r) = \frac{r\,P'}{f^2}, \tag{58}$$

$$\alpha_f(r) = \frac{r^2}{f}\,\frac{d}{dr}\left(\frac{f}{r}\right). \tag{59}$$

It is clear from Eqs. (37), (43), and (57) that $j^{\,r} = j^{\,\theta} = j^{\,\phi} = 0$ in the vacuum region, $r \geq a$, which is characterized by $\alpha_g = \alpha_p = 0$. On the other hand, the contravariant components of the perturbed plasma current are clearly non-zero throughout the plasma.

Finally, Eqs. (50) and (56) yield the *axisymmetric ideal-MHD partial differential equations (p.d.e.s)*,

$$r\,\frac{\partial y}{\partial r} = \frac{\mathcal{Z}}{|\nabla r|^2} - \frac{r\,\nabla r\cdot\nabla\theta}{|\nabla r|^2}\,\frac{\partial y}{\partial\theta}, \tag{60}$$

$$r\,\frac{\partial\mathcal{Z}}{\partial r} = -\left[(\alpha_f\,\alpha_p + r\,\alpha_p')R^2 + q\,r\,\alpha_g' + r^2\,\alpha_g^2\right]y - \frac{\partial}{\partial\theta}\left(\frac{1}{|\nabla r|^2\,R^2}\,\frac{\partial y}{\partial\theta}\right) - \frac{\partial}{\partial\theta}\left(\frac{r\,\nabla r\cdot\nabla\theta}{|\nabla r|^2}\,\mathcal{Z}\right), \tag{61}$$

which govern the perturbed equilibrium.

### B. Derivation of the Axisymmetric Ideal-MHD O.D.E.s

Let

$$y(r,\theta) = \sum_m y_m(r)\, \mathrm{e}^{\,\mathrm{i}\, m\,\theta}, \tag{62}$$

$$\mathcal{Z}(r,\theta) = \sum_m Z_m(r)\, \mathrm{e}^{\,\mathrm{i}\, m\,\theta}. \tag{63}$$

Here, the $m$ are the set of (integer, but not necessarily positive) poloidal mode numbers included in the calculation. Equations (60) and (61) yield the *axisymmetric ideal-MHD ordinary differential equations (o.d.e.s)*:

$$r\,\frac{dy_m}{dr} = \sum_{m'} \left( A_m^{m'}\, Z_{m'} + B_m^{m'}\, y_{m'} \right), \tag{64}$$

$$r\,\frac{dZ_m}{dr} = \sum_{m'} \left( C_m^{m'}\, Z_{m'} + D_m^{m'}\, y_{m'} \right), \tag{65}$$

where

$$A_m^{m'} = c_m^{m'}, \tag{66}$$

$$B_m^{m'} = -m'\, f_m^{m'}, \tag{67}$$

$$C_m^{m'} = -m\, f_m^{m'}, \tag{68}$$

$$D_m^{m'} = -(\alpha_f\, \alpha_p + r\, \alpha_p')\, a_m^{m'} - (q\, r\, \alpha_g' + r^{\,2}\, \alpha_g^{\,2})\, \delta_m^{m'} + m\, m'\, b_m^{m'}, \tag{69}$$

and

$$a_m^{m'}(r) = \oint R^{\,2}\, \exp[-\mathrm{i}\,(m-m')\,\theta]\, \frac{d\theta}{2\pi}, \tag{70}$$

$$b_m^{m'}(r) = \oint |\nabla r|^{-2}\, R^{-2}\, \exp[-\mathrm{i}\,(m-m')\,\theta]\, \frac{d\theta}{2\pi}, \tag{71}$$

$$c_m^{m'}(r) = \oint |\nabla r|^{-2}\, \exp[-\mathrm{i}\,(m-m')\,\theta]\, \frac{d\theta}{2\pi}, \tag{72}$$

$$f_m^{m'}(r) = \oint \frac{\mathrm{i}\, r\, \nabla r \cdot \nabla\theta}{|\nabla r|^2}\, \exp[-\mathrm{i}\,(m-m')\,\theta]\, \frac{d\theta}{2\pi}. \tag{73}$$

Here, $\delta_m^{m'}$ is a Kronecker delta symbol. Note that $Z_0$ is independent of $r$ in the vacuum region, $r \geq a$, in which $\alpha_g = \alpha_p = 0$.

The axisymmetric ideal-MHD o.d.e.s play the same role for axisymmetric perturbations that the outer-region o.d.e.s, (102) and (103) of Ref. 11, play for non-axisymmetric perturbations. The main difference is that there are no singularities in the axisymmetric ideal-MHD o.d.e.s because an axisymmetric perturbation does not resonate with the plasma. In other words, there are no equilibrium flux-surfaces in the plasma at which $\mathbf{k}\cdot\mathbf{B}=0$, where $\mathbf{k}$ is the wavevector of the perturbation. This is because $|B^\theta(r)|>0$ throughout a conventional tokamak plasma equilibrium.

### C. Properties of Axisymmetric Ideal-MHD O.D.E.s

Note that $a^m_{m'}=a^{m'*}_m$, $b^m_{m'}=b^{m'*}_m$, $c^m_{m'}=c^{m'*}_m$, and $f^m_{m'}=-f^{m'*}_m$, which implies that

$$A^m_{m'}=A^{m*}_{m'}, \tag{74}$$

$$B^m_{m'}=-C^{m*}_{m'}, \tag{75}$$

$$C^m_{m'}=-B^{m*}_{m'}, \tag{76}$$

$$D^m_{m'}=D^{m*}_{m'}. \tag{77}$$

It follows from Eqs. (64), (65), and (74)–(77) that

$$r\,\frac{d}{dr}\left[\sum_m (Z_m\,y^*_m-y_m\,Z^*_m)\right]=0. \tag{78}$$

Thus, checking that $\sum_m(Z_m\,y^*_m-y_m\,Z^*_m)$ is indeed constant throughout the plasma is a good numerical check on the accuracy of the TJ code.

### D. Perturbed Electric Field

Suppose that all perturbed quantities vary in time as $\mathrm{e}^{-\mathrm{i}\,\omega\,t}$. Let $\mathbf{e}$ be the perturbed electric field, which satisfies

$$\nabla\times\mathbf{e}=\mathrm{i}\,\omega\,\mathbf{b}. \tag{79}$$

Hence,

$$e_\phi=\mathrm{i}\,\omega\,y, \tag{80}$$

and

$$\frac{\partial e_\theta}{\partial r} - \frac{\partial e_r}{\partial \theta} = -\mathrm{i}\,\omega\, r\,\alpha_g\, y, \tag{81}$$

where use has been made of Eqs. (24), (26), and (53). We also expect $\nabla \cdot \mathbf{e} = 0$, which implies that $e_r = e_\theta = 0$ in the vacuum region, $r \geq a$, in which $\alpha_g = 0$.

### E. Toroidal Electromagnetic Torque

The net toroidal electromagnetic torque exerted on the region of the plasma lying within the magnetic flux-surface whose label is $r$ is [11]

$$T_\phi(r) = \oint\oint r\, R^2\, b_\phi\, b^r\, d\theta\, d\phi. \tag{82}$$

It follows from Eqs. (24) and (42) that

$$T_\phi(r) = -\pi\,\alpha_g \oint \left(y^*\,\frac{\partial y}{\partial \theta} + y\,\frac{\partial y^*}{\partial \theta}\right) d\theta = -\pi\,\alpha_g \oint \frac{\partial |y|^2}{\partial \theta}\, d\theta = 0. \tag{83}$$

We conclude, not surprisingly, that an axisymmetric perturbation is incapable of exerting a net toroidal electromagnetic torque on the plasma.

In Ref. 12, the conservation of toroidal angular momentum is used to prove that the plasma and vacuum perturbed potential energy matrices are Hermitian. The fact that the toroidal electromagnetic torque is automatically zero in the axisymmetric case negates this proof. Hence, we need to find a new conserved quantity that does not automatically take the value zero. The electromagnetic energy flux is found to play this role.

### F. Electromagnetic Energy Flux

The net flux of electromagnetic energy across the plasma-vacuum interface is

$$\begin{aligned}\mathcal{E} &= \left[\oint\oint (\mathbf{e}\times\mathbf{b})\cdot\nabla r\,\mathcal{J}\,d\theta\,d\phi\right]_{r=a} = \left[\oint\oint (e_\theta\, b_\phi - e_\phi\, b_\theta)\,d\theta\,d\phi\right]_{r=a}\\ &= \mathrm{i}\,\pi\,\omega\oint (y\,\mathcal{Z}^* - y^*\,\mathcal{Z})_{r=a}\,d\theta = \mathrm{i}\,\pi^2\,\omega\sum_m (Z_m^*\,y_m - y_m^*\,Z_m)_{r=a}.\end{aligned} \tag{84}$$

Here, use has been made of Eqs. (52), (62), (63), and (80), as well as the fact that $e_\theta = 0$ for $r \geq a$.

### G. Perturbed Plasma Potential Energy

The perturbed plasma potential energy in the region of the plasma lying within the magnetic flux-surface whose label is $r$ is [12,19]

$$\delta W_p = \frac{1}{2} \oint \oint r\, R^2\, \xi^{r*} (-\mathbf{B}\cdot\mathbf{b} + \xi^r\, P')\, d\theta\, d\phi. \tag{85}$$

However,

$$\mathbf{B}\cdot\mathbf{b} - \xi^r\, P' = B^\theta\, b_\theta + B^\phi\, b_\phi - \xi^r\, P' = -\frac{f}{r\, R^2}\left(\mathcal{Z} + q\,\alpha_g\, y + \alpha_p\, R^2\right), \tag{86}$$

where use has been made of Eqs. (3)–(6), (25), (42), (52), and (58). Hence, we obtain

$$\delta W_p(r) = \frac{1}{2} \oint \oint y^* \left[\mathcal{Z} + (q\,\alpha_g + \alpha_p\, R^2)\, y\right] d\theta\, d\phi = \pi^2 \sum_m y_m^*\, \chi_m, \tag{87}$$

where

$$\chi_m(r) = Z_m + q\,\alpha_g\, y_m + \alpha_p \sum_{m'} a_m^{m'}\, y_{m'}. \tag{88}$$

## IV. GENERAL VACUUM SOLUTION

### A. Toroidal Coordinates

Let $\mu$, $\eta$, $\phi$ be right-handed *orthogonal toroidal coordinates* defined such that [11,12,20]

$$R = \frac{\sinh\mu}{\cosh\mu - \cos\eta}, \tag{89}$$

$$Z = \frac{\sin\eta}{\cosh\mu - \cos\eta}. \tag{90}$$

The scale-factors of the toroidal coordinate system are

$$h_\mu = h_\eta = \frac{1}{\cosh\mu - \cos\eta} \equiv h, \tag{91}$$

$$h_\phi = \frac{\sinh\mu}{\cosh\mu - \cos\eta} = h\, \sinh\mu. \tag{92}$$

Moreover,

$$\mathcal{J}' \equiv (\nabla\mu \times \nabla\eta \cdot \nabla\phi)^{-1} = h^3\, \sinh\mu. \tag{93}$$

### B. Perturbed Magnetic Field

The curl-free perturbed magnetic field in the vacuum region is written $\mathbf{b} = \mathrm{i}\,\nabla V$, where $\nabla^2 V = 0$. The most general axisymmetric solution to Laplace's equation is [12,21]

$$V(z,\eta) = \sum_m (z - \cos\eta)^{1/2}\, U_m(z)\, \mathrm{e}^{-\mathrm{i}\,m\,\eta}, \tag{94}$$

$$U_m(z) = p_m\, \hat{P}_{|m|-1/2}(z) + q_m\, \hat{Q}_{|m|-1/2}(z), \tag{95}$$

where $z = \cosh\mu$, the $p_m$ and $q_m$ are arbitrary complex coefficients, and

$$\hat{P}_{|m|-1/2}(z) = \cos(|m|\,\pi)\, \frac{\sqrt{\pi}\,\Gamma(|m|+1/2)\,a^{\,|m|}}{2^{\,|m|-1/2}\,|m|!}\, P_{|m|-1/2}(z), \tag{96}$$

$$\hat{Q}_{|m|-1/2}(z) = \cos(|m|\,\pi)\, \frac{2^{\,|m|-1/2}\,|m|!}{\sqrt{\pi}\,\Gamma(|m|+1/2)\,a^{\,|m|}}\, Q_{|m|-1/2}(z). \tag{97}$$

Here, the $P_{|m|-1/2}(z)$ and $Q_{|m|-1/2}(z)$ are toroidal functions,[22] and $\Gamma(z)$ is a gamma function.[23]

### C. Toroidal Electromagnetic Angular Momentum Flux

The outward flux of toroidal angular momentum across a constant-$z$ surface is [11,12]

$$T_\phi(z) = -\oint\oint \mathcal{J}'\, b_\phi\, b^\mu\, d\eta\, d\phi = 0, \tag{98}$$

because $b_\phi = \mathrm{i}\,\partial V/\partial\phi = 0$. Of course, the flux has to be zero because the flux of angular momentum across the plasma-vacuum interface is zero, and there are no sources of angular momentum in the vacuum region surrounding the plasma. (See Sect. III E.)

### D. Electromagnetic Energy Flux

The outward flux of electromagnetic energy flux across a constant-$z$ surface is

$$\mathcal{E}(z) = -\oint\oint \mathcal{J}'\, \mathbf{e}\times\mathbf{b}\cdot\nabla\mu\, d\eta\, d\phi = -\mathrm{i}\,\pi \oint \left(e_\phi\,\frac{\partial V^*}{\partial\eta} - e_\phi^*\,\frac{\partial V}{\partial\eta}\right) d\eta, \tag{99}$$

given that $e_\mu = e_\eta = 0$ in the vacuum. However, $\nabla\times\mathbf{e} = \mathrm{i}\,\omega\,\mathbf{b}$ implies that

$$\frac{\partial e_\phi}{\partial\eta} = -\omega\, h\, \sinh\mu\, \frac{\partial V}{\partial\mu} = -\omega\, h\, \sinh^2\mu\, \frac{\partial V}{\partial z}. \tag{100}$$

Thus,

$$\mathcal{E}(z) = \mathrm{i}\,\pi \oint \left(\frac{\partial e_\phi}{\partial \eta}\,V^* - \frac{\partial e_\phi^*}{\partial \eta}\,V\right) d\eta = -\mathrm{i}\,\pi\,\omega \oint h\,\sinh^2\mu \left(\frac{\partial V}{\partial z}\,V^* - \frac{\partial V^*}{\partial z}\,V\right) d\eta$$
$$= \mathrm{i}\,\pi^2\,\omega \sum_m (p_m\,q_m^* - q_m\,p_m^*)\,(z^2-1)\,\mathcal{W}(P_{|m|-1/2}, Q_{|m|-1/2}), \tag{101}$$

where $\mathcal{W}(f,g) = f\,dg/dz - g\,df/dz$. However,[24]

$$\mathcal{W}(P_{|m|-1/2}, Q_{|m|-1/2}) = \frac{1}{1-z^2}, \tag{102}$$

so

$$\mathcal{E}(z) = -\mathrm{i}\,\pi^2\,\omega \sum_m (p_m\,q_m^* - q_m\,p_m^*). \tag{103}$$

Note that $\mathcal{E}$ is independent of $z$, as must be the case because there are no energy sources in the vacuum region.

### E. Solution in Vacuum Region

In the large-aspect ratio limit, $r \ll 1$, it can be demonstrated that [24]

$$z \simeq \frac{1}{r}, \tag{104}$$

$$z^{\,1/2}\,\hat{P}_{-1/2}(z) \simeq \frac{1}{2}\ln(8\,z), \tag{105}$$

$$z^{1/2}\,\hat{P}_{|m|-1/2}(z) \simeq \frac{\cos(|m|\,\pi)\,(a\,z)^{|m|}}{|m|}, \tag{106}$$

$$z^{1/2}\,\hat{Q}_{|m|-1/2}(z) \simeq \frac{\cos(|m|\,\pi)\,(a\,z)^{-|m|}}{2}. \tag{107}$$

Note that Eq. (106) only applies to $|m| > 0$.

According to Eq. (24) and (52),

$$\frac{\partial y}{\partial \theta} = \mathcal{J}\,\mathbf{b}\cdot\nabla r = \mathrm{i}\,\mathcal{J}\,\nabla V\cdot\nabla r, \tag{108}$$

$$\mathcal{Z} = -\mathcal{J}\,\nabla\phi\times\nabla r\cdot\mathbf{b} = -\mathrm{i}\,\frac{\partial V}{\partial \theta}. \tag{109}$$

Now, we have already seen that $Z_0 \equiv \oint \mathcal{Z}\,d\theta/(2\pi) = 0$ is independent of $r$ in the vacuum region. (See Sect. III B.) However, it is clear that Eq. (109) mandates that this constant

value is zero. This constraint implies that the axisymmetric ideal modes to which the plasma equilibrium is subject do not change the net toroidal current flowing in the plasma. [See Eqs. (52) and (219).] Note, further, that $y_0 \equiv \oint y\, d\theta/(2\pi)$ does not influence the vacuum potential, $V(r,\theta)$.

The previous two equations yield [12]

$$\underline{V}(r) = \underline{\underline{\mathcal{P}}}(r)\,\underline{p} + \underline{\underline{\mathcal{Q}}}(r)\,\underline{q}, \tag{110}$$

$$\underline{\psi}(r) = \underline{\underline{\mathcal{R}}}(r)\,\underline{p} + \underline{\underline{\mathcal{S}}}(r)\,\underline{q}, \tag{111}$$

where $V(r,\theta) = \sum_m V_m(r)\,\mathrm{e}^{\,\mathrm{i}\,m\,\theta}$, $Z_m(r) = m\,V_m(r)$, $\psi_m(r) = m\,y_m(r)$, $\underline{V}(r)$ is the vector of the $V_m(r)$ values, $\underline{\psi}(r)$ is the vector of the $\psi_m(r)$ values, $\underline{\underline{\mathcal{P}}}(r)$ is the matrix of the

$$\mathcal{P}_{mm'}(r) = \oint_r (z-\cos\eta)^{1/2}\,\hat{P}_{|m'|-1/2}(z)\,\exp[-\mathrm{i}\,(m\,\theta + m'\,\eta)]\,\frac{d\theta}{2\pi} \tag{112}$$

values, $\underline{\underline{\mathcal{Q}}}(r)$ is the matrix of the

$$\mathcal{Q}_{mm'}(r) = \oint_r (z-\cos\eta)^{1/2}\,\hat{Q}_{|m'|-1/2}(z)\,\exp[-\mathrm{i}\,(m\,\theta + m'\,\eta)]\,\frac{d\theta}{2\pi} \tag{113}$$

values, $\underline{\underline{\mathcal{R}}}(r)$ is the matrix of the

$$\begin{aligned}\mathcal{R}_{mm'}(r) = \oint_r \Bigg\{ &\left[\frac{1}{2}\,(z-\cos\eta)^{-1/2}\,\hat{P}_{|m'|-1/2}(z) + (z-\cos\eta)^{1/2}\,\frac{d\hat{P}_{|m'|-1/2}}{dz}\right]\mathcal{J}\,\nabla r\cdot\nabla z\\ &+\left[\frac{1}{2}\,(z-\cos\eta)^{-1/2}\,\sin\eta - \mathrm{i}\,m'\,(z-\cos\eta)^{1/2}\right]\hat{P}_{|m'|-1/2}(z)\,\mathcal{J}\,\nabla r\cdot\nabla\eta\Bigg\}\\ &\times\exp[-\mathrm{i}\,(m\,\theta+m'\,\eta)]\,\frac{d\theta}{2\pi}\end{aligned} \tag{114}$$

values, $\underline{\underline{\mathcal{S}}}(r)$ is the matrix of the

$$\begin{aligned}\mathcal{S}_{mm'}(r) = \oint_r \Bigg\{ &\left[\frac{1}{2}\,(z-\cos\eta)^{-1/2}\,\hat{Q}_{|m'|-1/2}(z) + (z-\cos\eta)^{1/2}\,\frac{d\hat{Q}_{|m'|-1/2}}{dz}\right]\mathcal{J}\,\nabla r\cdot\nabla z\\ &+\left[\frac{1}{2}\,(z-\cos\eta)^{-1/2}\,\sin\eta - \mathrm{i}\,m'\,(z-\cos\eta)^{1/2}\right]\hat{Q}_{|m'|-1/2}(z)\,\mathcal{J}\,\nabla r\cdot\nabla\eta\Bigg\}\\ &\times\exp[-\mathrm{i}\,(m\,\theta+m'\,\eta)]\,\frac{d\theta}{2\pi}\end{aligned} \tag{115}$$

values, $\underline{p}$ is the vector of the $p_m$ coefficients, and $\underline{q}$ is the vector of the $q_m$ coefficients. Here, the subscript $r$ on the integrals indicates that they are taken at constant $r$.

### F. Energy Conservation

According to Eq. (84), the net flux of electromagnetic energy across the plasma-vacuum interface is

$$\mathcal{E} = \mathrm{i}\,\pi^2\,\omega\,(\underline{V}^\dagger\,\underline{\psi} - \underline{\psi}^\dagger\,\underline{V}). \tag{116}$$

However, energy conservation requires this flux to be equal to the energy flux through the vacuum region, so Eq. (103) gives

$$\mathcal{E} = -\mathrm{i}\,\pi^2\,\omega\,(\underline{q}^\dagger\,\underline{p} - \underline{p}^\dagger\,\underline{q}). \tag{117}$$

Equations (110), (111), and the previous two equations, yield [12]

$$\underline{\underline{\mathcal{P}}}^\dagger\,\underline{\underline{\mathcal{R}}} = \underline{\underline{\mathcal{R}}}^\dagger\,\underline{\underline{\mathcal{P}}}, \tag{118}$$

$$\underline{\underline{\mathcal{Q}}}^\dagger\,\underline{\underline{\mathcal{S}}} = \underline{\underline{\mathcal{S}}}^\dagger\,\underline{\underline{\mathcal{Q}}}, \tag{119}$$

$$\underline{\underline{\mathcal{P}}}^\dagger\,\underline{\underline{\mathcal{S}}} - \underline{\underline{\mathcal{R}}}^\dagger\,\underline{\underline{\mathcal{Q}}} = \underline{\underline{1}}. \tag{120}$$

It can also be demonstrated that

$$\underline{\underline{\mathcal{Q}}}\,\underline{\underline{\mathcal{P}}}^\dagger = \underline{\underline{\mathcal{P}}}\,\underline{\underline{\mathcal{Q}}}^\dagger, \tag{121}$$

$$\underline{\underline{\mathcal{R}}}\,\underline{\underline{\mathcal{S}}}^\dagger = \underline{\underline{\mathcal{S}}}\,\underline{\underline{\mathcal{R}}}^\dagger. \tag{122}$$

The previous five equations hold throughout the vacuum region.

### G. No-Wall Matching Condition

Suppose that the plasma is surrounded by a vacuum region that extends to infinity. In this case,

$$\underline{q} = \underline{0}, \tag{123}$$

because the $\underline{\underline{\mathcal{Q}}}(r)$ solutions blow up in an unphysical manner as $r \to \infty$. [See Eqs. (104) and (107)]. It immediately follows from Eq. (117) that

$$\mathcal{E} = 0. \tag{124}$$

In other words, as we would expect, there is zero net flux of electromagnetic energy out of a plasma surrounded by a vacuum region that extends to infinity (because there is nothing at infinity that could absorb the energy flux). Equations (110) and (111) imply that

$$\underline{V}(r = a_+) = \underline{\underline{H}}\,\underline{\psi}(r = a), \tag{125}$$

where

$$\underline{\underline{H}} = \underline{\underline{\mathcal{P}}}_a\,\underline{\underline{\mathcal{R}}}_a^{-1} \tag{126}$$

is termed the *no-wall vacuum matrix*. Here, $\underline{\underline{\mathcal{P}}}_a = \underline{\underline{\mathcal{P}}}(r = a)$, et cetera. Equation (118) ensures that $\underline{\underline{H}}$ is Hermitian.

### H. Perfect-Wall Matching Condition

Suppose that the plasma is surrounded by a vacuum region that is bounded by a perfectly conducting wall that is conformal to the plasma-vacuum interface, and whose inner surface lies at $r = b_w\,a$, where $b_w \geq 1$. Because the wall is perfectly conducting, $\underline{\psi}(r = b_w\,a) = 0$.[19] In other words, the normal component of the perturbed magnetic field is zero at the inner surface of the wall. It follows from Eq. (111) that

$$\underline{p} = -\underline{\underline{I}}_b\,\underline{q}, \tag{127}$$

where

$$\underline{\underline{I}}_b = \underline{\underline{\mathcal{R}}}_b^{-1}\,\underline{\underline{\mathcal{S}}}_b \tag{128}$$

is termed the *wall matrix*. Here, $\underline{\underline{\mathcal{R}}}_b = \underline{\underline{\mathcal{R}}}(r = b_w\,a)$, et cetera. Equation (122) ensures that $\underline{\underline{I}}_b$ is Hermitian. It immediately follows from Eq. (117) that

$$\mathcal{E} = 0. \tag{129}$$

In other words, as we would expect, there is zero net electromagnetic energy flux out of a plasma surrounded by a vacuum region that is bounded by perfectly conducting wall (because a perfect wall could not absorb the energy flux).

Making use of Eqs. (110) and (111), the matching condition at the plasma-vacuum interface for a perfectly-conducting wall becomes

$$\underline{V}(r=a_+) = \underline{\underline{G}}\,\underline{\psi}(r=a), \tag{130}$$

where

$$\underline{\underline{G}} = (\underline{\underline{\mathcal{Q}}}_a - \underline{\underline{\mathcal{P}}}_a\,\underline{\underline{I}}_b)\,(\underline{\underline{\mathcal{S}}}_a - \underline{\underline{\mathcal{R}}}_a\,\underline{\underline{I}}_b)^{-1} \tag{131}$$

is termed the *perfect-wall vacuum matrix*. It is easily demonstrated from Eqs. (118)–(120) that

$$\underline{\underline{G}} - \underline{\underline{G}}^\dagger = -[(\underline{\underline{\mathcal{S}}}_a - \underline{\underline{\mathcal{R}}}_a\,\underline{\underline{I}}_b)^{-1}]^\dagger\,(\underline{\underline{I}}_b - \underline{\underline{I}}_b^\dagger)\,(\underline{\underline{\mathcal{S}}}_a + \underline{\underline{\mathcal{R}}}_a\,\underline{\underline{I}}_b)^{-1}. \tag{132}$$

Thus, the vacuum matrix, $\underline{\underline{G}}$, is Hermitian because the wall matrix, $\underline{\underline{I}}_b$, is Hermitian.

## I. Perturbed Vacuum Potential Energy

Equation (24) implies that

$$\mathcal{J}\,\nabla r\cdot\nabla V = -\mathrm{i}\,\frac{\partial y}{\partial\theta}. \tag{133}$$

The perturbed potential energy in the vacuum region is [12,19]

$$\begin{aligned}
\delta W_v &= \frac{1}{2}\int_{a_+}^{\infty}\oint\oint \mathbf{b}^*\cdot\mathbf{b}\,\mathcal{J}\,dr\,d\theta\,d\phi = \frac{1}{2}\int_{a_+}^{\infty}\oint\oint \nabla V^*\cdot\nabla V\,\mathcal{J}\,dr\,d\theta\,d\phi\\
&= -\frac{1}{2}\left(\oint\oint \mathcal{J}\,\nabla r\cdot\nabla V^*\,V\,d\theta\,d\phi\right)_{a_+} = -\frac{1}{2}\left[\oint\oint\left(-\mathrm{i}\,\frac{\partial y}{\partial\theta}\right)^*\,V\,d\theta\,d\phi\right]_{a_+}\\
&= -\pi^2\left(\sum_m m\,y_m^*\,V_m\right)_{a_+},
\end{aligned} \tag{134}$$

where use has been made of the facts that $\nabla^2 V = 0$ and $\nabla r\cdot\nabla V = 0$ at the ideal wall.

## V. GENERAL IDEAL STABILITY

### A. Perturbed Plasma Potential Energy

Suppose that the poloidal harmonics included in the calculation range from $m = -m_{\max}$ to $m = m_{\max}$, where $m_{\max} > 0$. Let the $y_{mm'}(r)$ and the $Z_{mm'}(r)$ be linearly independent

solutions of the axisymmetric ideal-MHD o.d.e.s, (64) and (65), that are well-behaved at the magnetic axis. Here, $m$ indexes the poloidal harmonic, whereas $m'$ indexes the dominant poloidal harmonic close to the magnetic axis. (See Sect. VII H.) Let

$$\chi_{mm'}(r) = Z_{mm'} + q\,\alpha_g\,y_{mm'} + \alpha_p \sum_{m''} a_m^{m''}\,y_{m''m'}. \tag{135}$$

We can form $J = 2\,m_{\max}$ linearly independent solutions that all have $Z_0 = 0$ at $r = a$, as mandated by the matching condition (109). The most general solution to the axisymmetric ideal-MHD o.d.e.s that satisfied the constraint $Z_0(a) = 0$ is written

$$y_m(r) = \sum_{m'=1,J} y_{mm'}(r)\,\alpha_{m'}, \tag{136}$$

$$\chi_m(r) = \sum_{m'=1,J} \chi_{mm'}(r)\,\alpha_{m'}, \tag{137}$$

where the $\alpha_m$ are arbitrary complex coefficients. Here, $m$ indexes the poloidal harmonic and $m'$ indexes the solution. Note that $\chi_m(a_-) = Z_m(a_-) = 0$ because $\alpha_g(a) = \alpha_p(a) = 0$. [See Eq. (88).]

According to Eq. (87), the net perturbed plasma potential energy is

$$\delta W_p = \pi^2\,\underline{y}^\dagger\,\underline{\chi}, \tag{138}$$

where $\underline{y}$ is the vector of the $y_m(a)$ values, excluding the $m = 0$ harmonic, and $\underline{\chi}$ the vector of the $\chi_m(a_-)$ values, excluding the $m = 0$ harmonic. We can exclude the $m = 0$ harmonic because, by construction our solutions are such that $\chi_0(a_-) = 0$. It follows that

$$\delta W_p = \pi^2\,\underline{\alpha}^\dagger\,\underline{\underline{y}}^\dagger\,\underline{\underline{\chi}}\,\underline{\alpha}, \tag{139}$$

where $\underline{\alpha}$ is the vector of the $\alpha_m$ values, $\underline{\underline{y}}$ the matrix of the $y_{mm'}(a)$ values, excluding the $m = 0$ harmonic, and $\underline{\underline{\chi}}$ the matrix of the $\chi_{mm'}(a_-)$ values, excluding the $m = 0$ harmonic. If

$$\underline{\underline{\chi}} = \underline{\underline{W}}_p\,\underline{\underline{y}}. \tag{140}$$

then

$$\delta W_p = \pi^2\,\underline{\alpha}^\dagger\,\underline{\underline{y}}^\dagger\,\underline{\underline{W}}_p\,\underline{\underline{y}}\,\underline{\alpha}. \tag{141}$$

Equations (84), (124), and (129) imply that $\underline{\underline{W}}_p$ is Hermitian.

### B. Perturbed Vacuum Potential Energy

According to Eq. (134), the perturbed vacuum potential energy is

$$\delta W_v = -\pi^2 \sum_m m\, y_m^*(a)\, V_m(a_+), \tag{142}$$

excluding the $m = 0$ harmonic, which obviously does not affect the vacuum energy. However, Eqs. (125) and (130) imply that

$$V_m(a_+) = \sum_{m'} H_{mm'}\, m'\, y_{m'}(a) \tag{143}$$

in the no-wall case, and

$$V_m(a_+) = \sum_{m'} G_{mm'}\, m'\, y_{m'}(a) \tag{144}$$

in the perfect-wall case. Here, we have excluded the $m' = 0$ harmonic, which also obviously does not affect the vacuum energy. Hence, we can write

$$\delta W_v = \pi^2\, \underline{y}^\dagger\, \underline{\underline{W}}_v\, \underline{y}, \tag{145}$$

where $\underline{\underline{W}}_v$ is the matrix of the $-m\, H_{mm'}\, m'$ values in the no-wall case, excluding the $m = 0$ and $m' = 0$ harmonics, and the $-m\, G_{mm'}\, m'$ values in the perfect-wall case, likewise excluding the $m = 0$ and $m' = 0$ harmonics,. Given that $H_{mm'}$ and $G_{mm'}$ are Hermitian, we deduce that $\underline{\underline{W}}_v$ is Hermitian. It follows that

$$\delta W_v = \pi^2\, \underline{\alpha}^\dagger\, \underline{\underline{y}}^\dagger\, \underline{\underline{W}}_v\, \underline{\underline{y}}\, \underline{\alpha}. \tag{146}$$

### C. Total Perturbed Potential Energy

The total perturbed potential energy is

$$\delta W = \delta W_p + \delta W_v = \pi^2\, \underline{\alpha}^\dagger\, \underline{\underline{y}}^\dagger\, \underline{\underline{W}}\, \underline{\underline{y}}\, \underline{\alpha}, \tag{147}$$

where

$$\underline{\underline{W}} = \underline{\underline{W}}_p + \underline{\underline{W}}_v. \tag{148}$$

Given that $\underline{\underline{W}}_p$ and $\underline{\underline{W}}_v$ are both Hermitian, we deduce that $\underline{\underline{W}}$ is Hermitian.

### D. Ideal Stability

The fact that $\underline{\underline{W}}$ is Hermitian allows us to write

$$\underline{\underline{W}}\,\underline{\underline{\beta}} = \underline{\underline{\beta}}\,\underline{\underline{\Lambda}}, \tag{149}$$

$$\underline{\underline{\beta}}^{\dagger}\,\underline{\underline{\beta}} = \underline{\underline{1}}, \tag{150}$$

where $\underline{\underline{\beta}}$ is real, and $\underline{\underline{\Lambda}}$ is the diagonal matrix of the real $\lambda_m$ values. If $\underline{\hat{\alpha}} = \underline{\underline{\beta}}^{\dagger}\,\underline{y}\,\underline{\alpha}$ then

$$\delta W = \pi^2\,\underline{\hat{\alpha}}^{\dagger}\,\underline{\underline{\Lambda}}\,\underline{\hat{\alpha}} = \pi^2 \sum_{m=1,J} |\hat{\alpha}_m|^2\,\lambda_m. \tag{151}$$

Thus, if any of the $\lambda_m$ are negative then solutions exist for which $\delta W$ is negative, and the plasma is consequently unstable to an axisymmetric ideal mode.[19]

Suppose that $\sum_m |\hat{\alpha}_m|^2 = 1$. The ideal energy of the $m$th mode, for which $\hat{\alpha}_{m'} = \delta_{mm'}$, is

$$\delta W_m = \pi^2\,\lambda_m. \tag{152}$$

However,

$$\underline{\underline{\Lambda}} = \underline{\underline{\beta}}^{\dagger}\,\underline{\underline{W}}\,\underline{\underline{\beta}}, \tag{153}$$

Thus, the diagonal components of $\underline{\underline{\beta}}^{\dagger}\,\underline{\underline{W}}_p\,\underline{\underline{\beta}}$ and $\underline{\underline{\beta}}^{\dagger}\,\underline{\underline{W}}_v\,\underline{\underline{\beta}}$ are the plasma and vacuum contributions to the $\lambda_m$, respectively. The eigenfunction of the $m$th mode is conveniently normalized such that $y_{m'}(a) = \beta_{m'm}$.

## VI. GENERAL RESISTIVE WALL MODE STABILITY

The unnormalized minor radius of the wall is $b = b_w\,\bar{a}$, where $\bar{a} = \epsilon\,R_0$ is the unnormalized minor radius of the plasma. Suppose that the wall is resistive, and possesses an (unnormalized) electrical conductivity $\sigma_w$, as well as an (unnormalized) uniform radial thickness $d$. Consider a particular axisymmetric ideal mode for which the total perturbed potential energy in the absence of a wall, $\delta W_{nw}$, is negative, but the total perturbed potential energy in the presence of a perfectly conducting wall, $\delta W_{pw}$, is positive. In this case, the no-wall ideal mode is unstable (because $\delta W_{nw} < 0$). In the absence of the wall, this mode would grow

very rapidly on an Alfvénic timescale. On the other hand, the mode is completely stabilized if the wall is perfectly conducting (because $\delta W_{pw} > 0$). However, because the wall is not perfectly conducting, the unstable ideal mode is instead converted into a much more slowly growing *resistive wall mode*.

Let the (unnormalized) growth-rate of the resistive wall mode be

$$\gamma = \frac{\hat{\gamma}}{\tau_w}, \tag{154}$$

where

$$\tau_w = \mu_0 \, \sigma_w \, b \, d \tag{155}$$

is the (unnormalized) L/R time of the wall. The normalized growth-rate of the resistive wall mode is specified by [25,26]

$$\sqrt{\frac{\hat{\gamma}}{\delta_w}} \tanh\left(\sqrt{\delta_w \, \hat{\gamma}}\right) = -\frac{\delta W_{nw}}{\alpha_w \, \delta W_{pw}}, \tag{156}$$

where $\delta_w = d/b$, and

$$\alpha_w = \frac{(1/2) \int |\mathbf{A}_{nw} \times \mathbf{n}_w|^2 \, dS_w}{\epsilon \, b_w \, (\delta W_{v\,pw} - \delta W_{v\,nw})}. \tag{157}$$

Here, $\delta W_{v\,nw}$ is the vacuum potential energy in the absence of a wall, whereas $\delta W_{n\,pw}$ is the vacuum energy in the presence of a perfectly conducting wall. Moreover, $dS_w$ is an element of the inner surface of the wall, and the integral is over the whole inner surface. Furthermore, the perturbed magnetic field in the vacuum region, in the no-wall case, is written $\nabla \times \mathbf{A}_{nw}$. It is easily demonstrated from Eqs. (24) and (26) that $\mathbf{A}_{nw} = \sum_m y_{m\,nw}(r) \, \mathrm{e}^{\,\mathrm{i}\,m\,\theta} \, \nabla\phi$, where the $y_{m\,nw}(r)$ are the $y$-components of the no-wall eigenfunction of the mode in question. Finally, $dS_w = \mathcal{J} \, d\theta \, d\phi$. Hence, we deduce that

$$\alpha_w = \frac{\pi^2 \left(\sum_{m\neq 0} |y_{m\,nw}|^2\right)_{\hat{r}=b_w}}{\delta W_{v\,pw} - \delta W_{v\,nw}}. \tag{158}$$

Here, we have neglected $y_{0\,nw}$ because $y_0$ does not affect the vacuum energy.

Given that $\underline{q} = \underline{0}$ for a no-wall solution, Eq. (111) yields

$$\underline{\underline{m}} \, \underline{y}_b = \underline{\underline{\mathcal{R}}}_b \, \underline{\underline{\mathcal{R}}}_a^{-1} \, \underline{\underline{m}} \, \underline{y}_a, \tag{159}$$

which enables us to determine the $y_{m\neq 0\,nw}(\hat{r}=b_w)$ from the $y_{m\neq 0\,nw}(\hat{r}=1)$. Here, $\underline{\underline{m}}$ is the diagonal matrix of the poloidal mode numbers.

Finally, in the *thin-wall* limit, $\delta_w \ll 1$, Eq. (156) simplifies to give

$$\hat{\gamma} = -\frac{\delta W_{nw}}{\alpha_w\,\delta W_{pw}}. \tag{160}$$

## VII. INVERSE ASPECT-RATIO EXPANDED TOKAMAK EQUILIBRIUM

### A. Introduction

Up to now, our analysis has been completely general. At this stage, we introduce the simplifying approximation of an inverse aspect-ratio expanded plasma equilibrium.

### B. Equilibrium Magnetic Flux-Surfaces

Let us assume that the inverse aspect-ratio of the plasma, $\epsilon = a/R_0 = a$ (since $R_0$ is normalized to unity), is such that $0 < \epsilon \ll 1$. Let $r = \epsilon\,\hat{r}$, $\nabla = \epsilon^{-1}\,\hat{\nabla}$, and $' \rightarrow \epsilon^{-1}\,'$. Suppose that the loci of the equilibrium magnetic flux-surfaces can be written in the parametric form:[11,12,16]

$$R(\hat{r},\omega) = 1 - \epsilon\,\hat{r}\,\cos\omega + \epsilon^2 \sum_{j>0} H_j(\hat{r})\,\cos[(j-1)\,\omega] + \epsilon^2 \sum_{j>1} V_j(\hat{r})\,\sin[(j-1)\,\omega]$$
$$+ \epsilon^3\,L(\hat{r})\,\cos\omega, \tag{161}$$

$$Z(\hat{r},\omega) = \epsilon\,\hat{r}\,\sin\omega + \epsilon^2 \sum_{j>1} H_j(\hat{r})\,\sin[(j-1)\,\omega] - \epsilon^2 \sum_{j>1} V_j(\hat{r})\,\cos[(j-1)\,\omega]$$
$$- \epsilon^3\,L(\hat{r})\,\sin\omega, \tag{162}$$

where $j$ is a positive integer. Here, $H_1(\hat{r})$ controls the relative horizontal locations of the flux-surface centroids, $H_2(\hat{r})$ and $V_2(\hat{r})$ control the magnitudes and vertical tilts of the flux-surface ellipticities, $H_3(\hat{r})$ and $V_3(\hat{r})$ control the magnitudes and vertical tilts of the flux-surface triangularities, et cetera, whereas $L(\hat{r})$ is a flux-surface re-labelling parameter. Moreover, $\omega(R,Z)$ is a poloidal angle that is distinct from $\theta$. Note that $V_1$ does not appear in Eq. (162)

because such a factor merely gives rise to a rigid vertical shift of the plasma that can be eliminated by a suitable choice of the origin of the flux-coordinate system.

Let

$$J(\hat{r},\omega) = \frac{1}{\epsilon^2}\left(\frac{\partial R}{\partial \omega}\frac{\partial Z}{\partial \hat{r}} - \frac{\partial R}{\partial \hat{r}}\frac{\partial Z}{\partial \omega}\right) \tag{163}$$

be the Jacobian of the $\hat{r}$, $\omega$ coordinate system. We can transform to the $\hat{r}$, $\theta$ coordinate system by writing

$$\theta(\hat{r},\omega) = 2\pi \int_0^\omega \frac{J(\hat{r},\tilde{\omega})}{R(\hat{r},\tilde{\omega})}\,d\tilde{\omega} \Bigg/ \oint \frac{J(\hat{r},\omega)}{R(\hat{r},\omega)}\,d\omega, \tag{164}$$

$$\hat{r} = \frac{1}{2\pi}\oint \frac{J(\hat{r},\omega)}{R(\hat{r},\omega)}\,d\omega. \tag{165}$$

This transformation ensures that

$$\frac{\partial \theta}{\partial \omega} = \frac{J}{\hat{r}\,R}, \tag{166}$$

and, hence, that

$$\mathcal{J} \equiv \frac{R}{\epsilon}\left(\frac{\partial R}{\partial \theta}\frac{\partial Z}{\partial \hat{r}} - \frac{\partial R}{\partial \hat{r}}\frac{\partial Z}{\partial \hat{r}}\right) = \epsilon\, R\, J\,\frac{\partial \omega}{\partial \theta} = r\,R^2, \tag{167}$$

in accordance with Eq. (1).

### C. Metric Elements

We can determine the metric elements of the flux-coordinate system by combining Eqs. (161)–(165). Evaluating the elements up to $\mathcal{O}(\epsilon)$, but retaining $\mathcal{O}(\epsilon^2)$ contributions to terms that are independent of $\omega$, we obtain,[11,12]

$$L(\hat{r}) = \frac{\hat{r}^3}{8} - \frac{\hat{r}\,H_1}{2} - \frac{1}{2}\sum_{j>1}(j-1)\,\frac{H_j^2}{\hat{r}} - \frac{1}{2}\sum_{j>1}(j-1)\,\frac{V_j^2}{\hat{r}}, \tag{168}$$

$$\begin{aligned}\theta = \omega &+ \epsilon\,\hat{r}\,\sin\omega - \epsilon\sum_{j>0}\frac{1}{j}\left[H_j' - (j-1)\,\frac{H_j}{\hat{r}}\right]\sin(j\,\omega)\\ &+ \epsilon\sum_{j>1}\frac{1}{j}\left[V_j' - (j-1)\,\frac{V_j}{\hat{r}}\right]\cos(j\,\omega),\end{aligned} \tag{169}$$

$$|\hat{\nabla}\hat{r}|^2 = 1 + 2\,\epsilon\sum_{j>0} H_j'\,\cos(j\,\theta) + 2\,\epsilon\sum_{j>1} V_j'\,\sin(j\,\theta)$$

$$+\epsilon^2\left(\frac{3\,\hat{r}^2}{4}-H_1+\frac{1}{2}\sum_{j>0}\left[H_j'^2+(j^2-1)\,\frac{H_j^2}{\hat{r}^2}\right]\right.$$
$$\left.+\frac{1}{2}\sum_{j>1}\left[V_j'^2+(j^2-1)\,\frac{V_j^2}{\hat{r}^2}\right]\right), \tag{170}$$

$$\hat{\nabla}\hat{r}\cdot\hat{\nabla}\theta=\epsilon\,\sin\theta-\epsilon\sum_{j>0}\frac{1}{j}\left[H_j''+\frac{H_j'}{\hat{r}}+(j^2-1)\,\frac{H_j}{\hat{r}^2}\right]\sin(j\,\theta)$$
$$+\epsilon\sum_{j>1}\frac{1}{j}\left[V_j''+\frac{V_j'}{\hat{r}}+(j^2-1)\,\frac{V_j}{\hat{r}^2}\right]\cos(j\,\theta), \tag{171}$$

$$R^2=1-2\,\epsilon\,\hat{r}\,\cos\theta-\epsilon^2\left(\frac{\hat{r}^2}{2}-\hat{r}\,H_1'-2\,H_1\right). \tag{172}$$

Here, $' \equiv d/d\hat{r}$. Moreover, we have made use of the fact that $V_j \propto H_j$, for $j>1$, because $V_j$ and $H_j$ satisfy the identical differential equations, (178) and (179).

### D. Expansion of Inverse Grad-Shafranov Equation

Let us write [11,12]

$$f(\hat{r})=\epsilon\,\frac{\hat{r}\,g}{q}, \tag{173}$$

$$g(\hat{r})=1+\epsilon^2\,g_2(\hat{r})+\epsilon^4\,g_4(\hat{r}), \tag{174}$$

$$P'(\hat{r})=\epsilon^2\,p_2'(\hat{r}), \tag{175}$$

where $q$, $g_2$, $g_4$, and $p_2$ are all $\mathcal{O}(1)$. Here, the safety-factor, $q(\hat{r})$, and the second-order plasma pressure gradient, $p_2'(\hat{r})$, are the two free flux-surface functions that characterize the plasma equilibrium.

Expanding the inverse Grad-Shafranov equation, (15), order by order in the small parameter $\epsilon$, making use of Eqs. (170)–(175), we obtain [11,12,27]

$$g_2'=-p_2'-\frac{\hat{r}}{q^2}\,(2-s), \tag{176}$$

$$H_1''=-(3-2\,s)\,\frac{H_1'}{\hat{r}}-1+\frac{2\,p_2'\,q^2}{\hat{r}}, \tag{177}$$

$$H_j''=-(3-2\,s)\,\frac{H_j'}{\hat{r}}+(j^2-1)\,\frac{H_j}{\hat{r}^2}\qquad\text{for } j>1, \tag{178}$$

$$V_j'' = -(3-2\,s)\,\frac{V_j'}{\hat{r}} + (j^2-1)\,\frac{V_j}{\hat{r}^{\,2}} \qquad \text{for } j>1, \tag{179}$$

$$g_4' = g_2\left[p_2' - \frac{\hat{r}}{q^2}\,(2-s)\right] - \frac{\hat{r}}{q}\,\Sigma + p_2'\left(\frac{\hat{r}^{\,2}}{2} + \frac{\hat{r}^{\,2}}{q^2} - 2\,H_1 - 3\,\hat{r}\,H_1'\right), \tag{180}$$

where $s = \hat{r}\,q'/q$ is the magnetic shear, and

$$\Sigma = \frac{S_2}{q} - \frac{2-s}{q}\,S_3 \tag{181}$$

$$S_1(\hat{r}) = \frac{1}{2}\sum_{j>0}\left[3\,H_j'^{\,2} - (j^2-1)\,\frac{H_j^2}{\hat{r}^2}\right] + \frac{1}{2}\sum_{j>1}\left[3\,V_j'^{\,2} - (j^2-1)\,\frac{V_j^2}{\hat{r}^2}\right], \tag{182}$$

$$S_2(\hat{r}) = \frac{3\,\hat{r}^{\,2}}{2} - 2\,\hat{r}\,H_1' + \sum_{j>0}\left[H_j'^{\,2} + 2\,(j^2-1)\,\frac{H_j'\,H_j}{\hat{r}} - (j^2-1)\,\frac{H_j^2}{\hat{r}^{\,2}}\right] + \sum_{j>1}\left[V_j'^{\,2} + 2\,(j^2-1)\,\frac{V_j'\,V_j}{\hat{r}} - (j^2-1)\,\frac{V_j^2}{\hat{r}^{\,2}}\right], \tag{183}$$

$$S_3(\hat{r}) = -\frac{3\,\hat{r}^{\,2}}{4} + \frac{\hat{r}^{\,2}}{q^2} + H_1 + S_1, \tag{184}$$

$$S_4(\hat{r}) = \frac{7\,\hat{r}^{\,2}}{4} - H_1 - 3\,\hat{r}\,H_1' + S_1. \tag{185}$$

Note that the relative horizontal shift of magnetic flux-surfaces, $-H_1$, otherwise known as the *Shafranov shift*, is driven by toroidicity [the second term on the right-hand side of Eq. (177)], and plasma pressure gradients (the third term). All of the other shaping terms (i.e., the $H_j$, for $j>1$, and the $V_j$) are driven by axisymmetric currents flowing in external magnetic field-coils.

Equations (38), (58), (59), and (173)–(175) yield [11]

$$\alpha_p(\hat{r}) = \frac{p_2'\,q^2}{\hat{r}}\left(1 - 2\,\epsilon^{\,2}\,g_2\right), \tag{186}$$

$$\alpha_g(\hat{r}) = \frac{q}{\hat{r}}\left(g_2' - \epsilon^{\,2}\,g_2\,g_2' + \epsilon^{\,2}\,g_4'\right), \tag{187}$$

$$\alpha_f(\hat{r}) = -s + \epsilon^{\,2}\,\hat{r}\,g_2'. \tag{188}$$

Finally, it follows from Eqs. (171) and (177)–(179) that

$$\hat{\nabla}\hat{r}\cdot\hat{\nabla}\theta = 2\,\epsilon\left[1 - \frac{p_2'\,q^2}{\hat{r}} + (1-s)\,\frac{H_1'}{\hat{r}}\right]\sin\theta$$

$$- 2\,\epsilon \sum_{j>1} \frac{1}{j} \left[ -(1-s)\,\frac{H_j'}{\hat{r}} + (j^2-1)\,\frac{H_j}{\hat{r}^{\,2}} \right] \sin(j\,\theta)$$
$$+ 2\,\epsilon \sum_{j>1} \frac{1}{j} \left[ -(1-s)\,\frac{V_j'}{\hat{r}} + (j^2-1)\,\frac{V_j}{\hat{r}^{\,2}} \right] \cos(j\,\theta). \tag{189}$$

### E. Calculation of Coupling Coefficients

Equations (170) and (182) yield

$$|\hat{\nabla}\hat{r}|^{-2} = 1 - 2\,\epsilon \sum_{j>0} H_j'\,\cos(j\,\theta) - 2\,\epsilon \sum_{j>0} V_j' \sin(j\,\theta) + \epsilon^2 \left( -\frac{3\,\hat{r}^{\,2}}{4} + H_1 + S_1 \right), \tag{190}$$

Equation (172) gives

$$R^{-2} = 1 + 2\,\epsilon\,\hat{r}\,\cos\theta + \epsilon^2 \left( \frac{5\,\hat{r}^{\,2}}{2} - \hat{r}\,H_1' - 2\,H_1 \right). \tag{191}$$

The previous two equations imply that

$$|\hat{\nabla}\hat{r}|^{-2}\,R^{-2} = 1 + 2\,\epsilon\,\hat{r}\,\cos\theta - 2\,\epsilon \sum_{j>0} H_j'\,\cos(j\,\theta) - 2\,\epsilon \sum_{>1} V_j'\,\sin(j\,\theta)$$
$$+ \epsilon^2 \left( \frac{7\,\hat{r}^{\,2}}{4} - H_1 - 3\,\hat{r}\,H_1' + S_1 \right). \tag{192}$$

Finally, Eqs. (189) and (190) yield

$$\hat{\nabla}\hat{r}\cdot\hat{\nabla}\theta\,|\hat{\nabla}\hat{r}|^{-2} = 2\,\epsilon \left[ 1 - \frac{p_2'\,q^2}{\hat{r}} + (1-s)\,\frac{H_1'}{\hat{r}} \right] \sin\theta$$
$$- 2\,\epsilon \sum_{j>1} \frac{1}{j} \left[ -(1-s)\,\frac{H_j'}{\hat{r}} + (j^2-1)\,\frac{H_j}{\hat{r}^{\,2}} \right] \sin(j\,\theta)$$
$$+ 2\,\epsilon \sum_{j>1} \frac{1}{j} \left[ -(1-s)\,\frac{V_j'}{\hat{r}} + (j^2-1)\,\frac{V_j}{\hat{r}^{\,2}} \right] \cos(j\,\theta), \tag{193}$$

where use has been made of the fact that $V_j(\hat{r}) \propto H_j(\hat{r})$ for $j > 1$.

Equations (70)–(73), (172), (190), (192), and (193) imply that

$$a_m^{\,m'} = \delta_m^{\,m'} - \epsilon\,\hat{r}\,(\delta_{m'-m-1} + \delta_{m'-m+1}) - \epsilon^2 \left( \frac{\hat{r}^{\,2}}{2} - \hat{r}\,H_1' - 2\,H_1 \right) \delta_m^{\,m'}, \tag{194}$$

$$b_m^{\,m'} = \delta_m^{\,m'} + \epsilon\,\hat{r}\,(\delta_{m'-m-1} + \delta_{m'-m+1}) - \epsilon \sum_{j>0} H_j'\,(\delta_{m'-m-j} + \delta_{m'-m+j})$$

$$- \epsilon \sum_{j>1} \mathrm{i}\, V_j' \,(\delta_{m'-m-j} - \delta_{m'-m+j}) + \epsilon^2 \left( \frac{7\,\hat{r}^{\,2}}{4} - H_1 - 3\,\hat{r}\,H_1' + S_1 \right) \delta_m^{m'}, \tag{195}$$

$$c_m^{m'} = \delta_m^{m'} - \epsilon \sum_{j>0} H_j' \,(\delta_{m'-m-j} + \delta_{m'-m+j}) - \epsilon \sum_{j>1} \mathrm{i}\, V_j' \,(\delta_{m'-m-j} - \delta_{m'-m+j})$$
$$+ \epsilon^2 \left( -\frac{3\,\hat{r}^{\,2}}{4} + H_1 + S_1 \right) \delta_m^{m'}, \tag{196}$$

$$f_m^{m'} = -\epsilon \left[ \hat{r} - p_2'\, q^2 + (1-s)\, H_1' \right] (\delta_{m'-m-1} - \delta_{m'-m+1})$$
$$+ \epsilon \sum_{j>1} \frac{1}{j} \left[ -(1-s)\, H_j' + (j^2-1)\, \frac{H_j}{\hat{r}} \right] (\delta_{m'-m-j} - \delta_{m'-m+j})$$
$$+ \epsilon \sum_{j>1} \frac{\mathrm{i}}{j} \left[ -(1-s)\, V_j' + (j^2-1)\, \frac{V_j}{\hat{r}} \right] (\delta_{m'-m-j} + \delta_{m'-m+j}). \tag{197}$$

If we write

$$\alpha_g = \alpha_g^{(0)} + \epsilon^2\, \alpha_g^{(2)}, \tag{198}$$

$$\alpha_p = \alpha_p^{(0)} + \epsilon^2\, \alpha_p^{(2)}, \tag{199}$$

$$\alpha_f = \alpha_f^{(0)} + \epsilon^2\, \alpha_f^{(2)}, \tag{200}$$

$$a_m^{m'} = 1 + \epsilon\, a_m^{m'\,(1)} + \epsilon^2\, a_m^{m'\,(2)}, \tag{201}$$

$$b_m^{m'} = 1 + \epsilon\, b_m^{m'\,(1)} + \epsilon^2\, b_m^{m'\,(2)}, \tag{202}$$

$$D_m^{m'} = D_m^{m'\,(0)} + \epsilon\, D_m^{m'\,(1)} + \epsilon^2\, D_m^{m'\,(2)}, \tag{203}$$

where $\alpha_g^{(0)}$, $\alpha_g^{(2)}$, et cetera, are $\mathcal{O}(1)$, then it follows from Eq. (69) that

$$D_m^{m\,(0)} = -\alpha_f^{(0)}\, \alpha_p^{(0)} - \hat{r}\, \alpha_p'^{(0)} - q\,\hat{r}\, \alpha_g'^{(0)} + m^2, \tag{204}$$

$$D_m^{m'\,(1)} = -\left[ \alpha_f^{(0)}\, \alpha_p^{(0)} + \hat{r}\, \alpha_p'^{(0)} \right] a_m^{m'\,(1)} + m\, m'\, b_m^{m'\,(1)}, \tag{205}$$

$$D_m^{m\,(2)} = -\left[ \alpha_f^{(0)}\, \alpha_p^{(0)} + \hat{r}\, \alpha_p'^{(0)} \right] a_m^{m'\,(2)} - \alpha_f^{(0)}\, \alpha_p^{(2)} - \alpha_f^{(2)}\, \alpha_p^{(0)} - \hat{r}\, \alpha_p'^{(2)} - q\,\hat{r}\, \alpha_g'^{(2)}$$
$$- \hat{r}^{\,2} \left[ \alpha_g^{(0)} \right]^2 + m^2\, b_m^{m\,(2)}. \tag{206}$$

Finally, Eqs. (70)–(73), (194)–(197), and (204)–(206) give the following expressions for the coupling coefficients appearing in the axisymmetric ideal-MHD o.d.e.s, (64) and (74):

$$A_m^m(\hat{r}) = 1 + \epsilon^2 \left( -\frac{3\,\hat{r}^{\,2}}{4} + H_1 + S_1 \right), \tag{207}$$

$$A_m^{m\pm1}(\hat{r}) = -\epsilon\, H_1', \tag{208}$$

$$A_m^{m\pm j}(\hat{r}) = -\epsilon\,(H_j' \pm \mathrm{i}\, V_j') \qquad \text{for } j > 1, \tag{209}$$

$$B_m^{m}(\hat{r}) = 0, \tag{210}$$

$$B_m^{m\pm1}(\hat{r}) = \pm\epsilon\,(m \pm 1)\left[\hat{r} - p_2'\, q^2 + (1-s)\, H_1'\right], \tag{211}$$

$$B_m^{m\pm j}(\hat{r}) = \pm\epsilon\,\frac{m \pm j}{j}\,\left[(1-s)\,(H_j' \pm \mathrm{i}\, V_j') - (j^2-1)\,\frac{H_j \pm \mathrm{i}\, V_j}{\hat{r}}\right] \qquad \text{for } j > 1, \tag{212}$$

$$C_m^{m}(\hat{r}) = 0, \tag{213}$$

$$C_m^{m\pm1}(\hat{r}) = \pm\epsilon\, m\left[\hat{r} - p_2'\, q^2 + (1-s)\, H_1'\right], \tag{214}$$

$$C_m^{m\pm j}(\hat{r}) = \pm\epsilon\,\frac{m}{j}\,\left[(1-s)\,(H_j' \pm \mathrm{i}\, V_j') - (j^2-1)\,\frac{H_j \pm \mathrm{i}\, V_j}{\hat{r}}\right] \qquad \text{for } j > 1, \tag{215}$$

$$\begin{aligned} D_m^{m}(\hat{r}) = {} & m^2 + q\,\hat{r}\,\frac{d}{d\hat{r}}\left(\frac{2-s}{q}\right) + \epsilon^2\, m^2\, S_4 \\ & + \epsilon^2\left\{-\hat{r}^{\,2}\left(\frac{2-s}{q}\right)^2 + q\,\hat{r}\,\frac{d\Sigma}{d\hat{r}} - \hat{r}\,\frac{d}{d\hat{r}}(\hat{r}\, p_2') - 2\,(1-s)\,\hat{r}\, p_2'\right. \\ & \left. + 2\,\hat{r}\, p_2'\, q^2\left(-2 + \frac{3\, p_2'\, q^2}{\hat{r}}\right) + 2\, H_1'\, q^2\left[\frac{d}{d\hat{r}}(\hat{r}\, p_2') - 4\,(1-s)\, p_2'\right]\right\}, \end{aligned} \tag{216}$$

$$D_m^{m\pm1}(\hat{r}) = \epsilon\, q^2\left[\frac{d}{d\hat{r}}(\hat{r}\, p_2') - (2-s)\, p_2'\right] + \epsilon\, m\,(m \pm 1)\,(\hat{r} - H_1'), \tag{217}$$

$$D_m^{m\pm j}(\hat{r}) = -\epsilon\, m\,(m \pm j)\,(H_j' \pm \mathrm{i}\, V_j') \qquad \text{for } j > 1. \tag{218}$$

Our system of equations is now complete.

### F. Toroidal Plasma Current

The net toroidal plasma current flowing in the plasma is given by

$$I_p = \oint_{r=a} \mathcal{J}\,\nabla\phi \times \nabla r \cdot \mathbf{B}\, d\theta = \oint_{r=a} B_\theta\, d\theta, \tag{219}$$

which yields

$$I_p = \gamma_{\mathrm{shape}}\, I_{p\,\mathrm{cly}}, \tag{220}$$

where

$$I_{p\,\mathrm{cyl}} = \frac{2\pi\, a^2\, g(a)}{q(a)} \tag{221}$$

is the plasma current predicted by cylindrical theory, whereas

$$\gamma_{\mathrm{shape}} = \oint_{r=a} |\hat{\nabla}\hat{r}|^2\, \frac{d\theta}{2\pi} \tag{222}$$

is the factor by which the toroidal current is increased due to the shaping of the plasma's poloidal boundary.

### G. Plasma Self-Inductance

The dimensionless self-inductance of the plasma is conventionally defined as [11]

$$l_i = \frac{2\int_0^1 \hat{r}\, f^2\, \langle |\hat{\nabla}\hat{r}|^2 \rangle\, d\hat{r}}{(f\, \langle |\hat{\nabla}\hat{r}|^2 \rangle)^2_{\hat{r}=1}}. \tag{223}$$

### H. Behavior Close to Magnetic Axis

When $\hat{r} \ll 1$, the well-behaved solution of the axisymmetric ideal-MHD o.d.e.s, (64) and (65), that is dominated by the poloidal harmonic whose poloidal mode number is $m$ is such that

$$y_m(\hat{r}) = \hat{r}^{\,|m|}, \tag{224}$$

$$Z_m(\hat{r}) = |m|\, \hat{r}^{\,|m|}, \tag{225}$$

with $y_{m'}(\hat{r}) = Z_{m'}(\hat{r}) = 0$ for $m' \neq 0$.

## VIII. RESULTS

### A. Model Equilibria

The model plasma equilibria used in the TJ code are characterized by

$$q_{\mathrm{cly}}(r) = \frac{q(0)\, \nu\, \hat{r}^{\,2}}{1 - (1 - \hat{r}^{\,2})^{\nu}}, \tag{226}$$

$$p_2(r) = (1 - \hat{r}^{\,2})^{\mu}. \tag{227}$$

Here, $q_{\rm cly}(r)$ is the lowest order (cylindrical) safety-factor profile, whose relation to the actual profile is explained in Ref. 28. The parameter $q(0)$ is the safety-factor on the magnetic axis, whereas the parameter $\nu$ is automatically adjusted to give a desired value of the safety-factor at the plasma boundary, $q(a)$. Moreover, $p_2(r)$ is the normalized pressure profile [see Eq. (175)], and $p_2(0)$ controls the central plasma pressure.

The shaping of the poloidal cross-section of the plasma is determined by three parameters. The first is $H_2(a)$, which controls the plasma elongation. The second is $H_3(a)$, which controls the plasma triangularity. The third is $V_2(a)$, which controls the vertical tilt of the plasma. All of the $H_j(a)$ for $j > 3$, and the $V_k(a)$ for $k > 2$, are set to zero. Note that, to lowest order, the plasma elongation is $\kappa = 1 + \epsilon\, H_2(a)$, whereas the plasma triangularity is $\delta = \epsilon\, H_3(a)$.[28] Moreover, the large aspect-ratio ordering scheme adopted in Sect. VII requires $H_2(a)$ and $H_3(a)$ to be, at most, $\mathcal{O}(1)$ quantities.

In summary, our model equilibria are controlled by nine parameters: $q(0)$, $q(a)$, $p_2(0)$, $\mu$, $H_2(a)$, $H_3(a)$ and $V_2(a)$, as well as the inverse aspect-ratio, $\epsilon$, and the relative wall radius, $b_w$.

### B. Plasma Elongation

Figure 1 shows the variation of the no-wall perturbed potential energy, $\delta W_{nw}$, the perfect-wall perturbed plasma energy, $\delta W_{pw}$, the plasma parameter, $\alpha_w$ [see Eq. (158)], and the normalized growth-rate of the unstable axisymmetric mode, $\hat{\gamma}$, with the elongation parameter, $H_2(a)$, for a series of non-triangular plasmas. Results are shown for $m_{\rm max} = 5$ (which implies that 11 poloidal harmonics are included in the calculation), and $m_{\rm max} = 10$ (which implies that 21 poloidal harmonics are included in the calculation). The fact that these results are identical demonstrates that the TJ calculation has achieved convergence with $m_{\rm max} = 5$. It can be seen that if the plasma cross-section is circular [i.e., if $H_2(a) = 0$] then the axisymmetric mode is stable. However, as soon as the plasma elongation parameter exceeds a very small threshold value the axisymmetric mode becomes unstable.

As is clear from Fig. 2, if the plasma is vertically elongated [i.e., if $H_2(a) > 0$] then the axisymmetric mode causes the plasma to displace vertically. On the other hand, if the plasma is horizontally elongated [i.e., if $H_2(a) < 0$] then the axisymmetric mode causes the plasma to displace horizontally. It should be noted that, while most tokamak plasmas are vertically elongated, J-TEXT plasmas are horizontally elongated, and are, indeed, found to be subject to a horizontal instability.[29]

Of course, the axisymmetric mode needs to be stabilized by means of active feedback. Practical feedback coils must be placed outside the vacuum vessel, which means that the response time of the feedback system is limited by the L/R time of the vessel, $\tau_w$. Realizable feedback systems cannot stabilize the axisymmetric mode if its normalized growth-rate, $\hat{\gamma} = \gamma\,\tau_w$, exceeds a threshold value that is estimated to be about 1.5.[14] It can be seen that the normalized growth-rates shown in Fig. 1 all lie below this threshold value.

### C. Inverse Aspect-Ratio

Figure 3 shows the variation of the no-wall perturbed potential energy, $\delta W_{nw}$, the perfect-wall perturbed plasma energy, $\delta W_{pw}$, the plasma parameter, $\alpha_w$, and the normalized growth-rate of the unstable vertical mode, $\hat{\gamma}$, with the inverse aspect-ratio, $\epsilon$, for a series of non-triangular plasma equilibria with various different values of the elongation parameter, $H_2(a)$. It can be seen that the growth-rate of the vertical mode initially exhibits a linear increase with increasing inverse aspect-ratio, but that this linear behavior eventually breaks down. Moreover, the breakdown occurs earlier for higher values of $H_2(a)$.

### D. Triangularity

Figure 4 shows the variation of the no-wall perturbed potential energy, $\delta W_{nw}$, the perfect-wall perturbed plasma energy, $\delta W_{pw}$, the plasma parameter, $\alpha_w$, and the normalized growth-rate of the unstable vertical mode, $\hat{\gamma}$, with the plasma triangularity parameter, $H_3(a)$, for a series of elongated plasma equilibria with various different values of the normalized central pressure, $p_2(0)$. It can be seen that positive triangularity (i.e., a D-shaped plasma

cross-section—see Fig. 5) has a stabilizing effect on the vertical mode, whereas negative triangularity has a destabilizing effect. Moreover, whereas positive triangularity plasmas exhibit a mild decrease in the growth-rate of the vertical mode with increasing plasma pressure, negative triangularity plasmas exhibit a strong increase.[30] This finding is significant because, whereas negative triangularity plasma possess many attractive features, such as ELM-free (edge localized mode) operation,[30] their increased susceptibility to the exceptionally dangerous vertical mode is a major drawback. Furthermore, as is clear from right panel of Fig. 5, having a highly conformal wall does not solve the vertical mode problem for negative triangularity plasmas.

### E. Wall Radius

Figure 6 shows the variation of the no-wall perturbed potential energy, $\delta W_{nw}$, the perfect-wall perturbed plasma energy, $\delta W_{pw}$, the plasma parameter, $\alpha_w$, and the normalized growth-rate of the unstable vertical mode, $\hat{\gamma}$, with the relative wall radius, $b_w$, for a series of elongated non-triangular plasma equilibria with various different values of the normalized central pressure, $p_2(0)$. It can be seen that the perfect-wall perturbed plasma energy becomes extremely positive as the wall approaches the plasma boundary (i.e., as $b_w \rightarrow 1$). This is indicative of the fact that a close-fitting perfectly conducting wall is capable of completely stabilizing any ideal external mode.[19] However, as is clear from the figure, a close-fitting wall does not stabilize the resistive wall mode. In fact, $\hat{\gamma}$ asymptotes to a finite positive value as $b_w \rightarrow 1$. On the other hand, the growth-rate of the resistive wall mode increases as the wall becomes more distant from the plasma, and quickly attains dangerous levels (i.e., comparable with 1.5). This finding is significant because the vacuum vessel in a tokamak fusion reactor is likely to be quite distant from the plasma because of the presence of shielding material inside the vessel.

### F. Internal Inductance

Figure 7 shows the variation of the no-wall perturbed potential energy, $\delta W_{nw}$, the perfect-wall perturbed plasma energy, $\delta W_{pw}$, the plasma parameter, $\alpha_w$, and the normalized growth-rate of the unstable vertical mode, $\hat{\gamma}$, with the normalized plasma internal inductance, $l_i$, for a series of elongated plasma equilibria with various different values of triangularity parameter, $H_3(a)$. In practice, the internal inductance is varied by changing $q(0)$ at fixed $q(a)$. It can be seen that while non-triangular plasmas only exhibit a weak dependence of the growth-rate of the vertical mode with $l_i$, triangular plasmas exhibit an increase in the growth-rate with increasing $l_i$ (i.e., increased peaking of the plasma current).

### G. Non Up-Down Symmetric Plasmas

A conventional tokamak plasma generally possess a single magnetic X-point, located either above or below the plasma, which renders it non up-down symmetric. We can model this effect by introducing a vertical tilt, $V_2(a)$, into an elongated, triangular plasma equilibrium. As shown in Fig. 9, the resulting equilibria have egg-shaped poloidal cross-sections. The equilibrium shown in the left panel is a rough model of a plasma with an upper X-point on the high-field side, whereas the equilibrium shown in the right panel is a model of a plasma with an upper X-point on the low-field side. Figure 8 shows the variation of the no-wall perturbed potential energy, $\delta W_{nw}$, the perfect-wall perturbed plasma energy, $\delta W_{pw}$, the plasma parameter, $\alpha_w$, and the normalized growth-rate of the unstable axisymmetric mode, $\hat{\gamma}$, with the vertical tilt parameter, $V_2(a)$, for a series of elongated plasma equilibria with various different values of triangularity parameter, $H_3(a)$. It can be seen that lack of up-down symmetry has a destabilizing effect on the axisymmetric mode. Moreover, as is clear from Fig. 9, in the presence of a vertical tilt, the axisymmetric mode is no longer a purely vertical mode. In fact, the plasma displacement associated with the mode is directed toward the apex of the egg-shaped boundary.

### H. Wall Thickness

All of the results shown up to now in this paper have assumed that the thickness of the wall is much less than its minor radius. In fact, as is clear from a comparison of Eqs. (156) and (160), the relationship between the true normalized resistive wall mode growth-rate, $\hat{\gamma}$, and the thin-wall normalized growth-rate, $\hat{\gamma}_{\rm thin}$, is simply

$$\sqrt{\frac{\hat{\gamma}}{\delta_w}}\,\tanh\left(\sqrt{\delta_w\,\hat{\gamma}}\right) = \hat{\gamma}_{\rm thin}, \tag{228}$$

Here, $\delta_w$ is the ratio of the wall thickness to the wall minor radius. As is clear from Fig. 10, the wall thickness has little influence on the normalized growth-rate of the vertical mode when the growth-rate lies well below the practical threshold value for feedback control, 1.5. On the other hand, finite wall thickness leads to a higher normalized growth-rate when the growth-rate is comparable with the threshold value. This finding suggests that finite wall thickness should be taken into account when calculating the maximum controllable plasma elongation of a tokamak plasma.

## IX. SUMMARY

In this paper, we have demonstrated how to calculate the stability of axisymmetric modes in an aspect-ratio expanded tokamak plasma equilibrium surrounded by a conformal resistive wall. The calculation of the stability of axisymmetric modes turns out to be significantly different to the calculation of the stability of non-axisymmetric ideal modes described in Refs. 11 and 12. In particular, the role of the toroidal angular momentum flux (which is identically zero for an axisymmetric mode) is instead played by the electromagnetic energy flux. The conservation of electromagnetic energy can be used to prove that the perturbed plasma potential energy matrix is Hermitian. The calculation described in the paper has been implemented in the TJ toroidal tearing mode code. The results of the enhanced TJ code are broadly similar to those reported in the literature.[14,30] In particular, positive triangularity is found to have a stabilizing effect on the vertical mode, whereas negative triangularity has a marked destabilizing effect. Lack of up-down symmetry is found to have a destabilizing

effect on the vertical mode. Finally, our calculations indicate that finite wall thickness should be taken into account when determining the maximum controllable plasma elongation of a tokamak plasma.

It should be noted that all of the analysis prior to Sect. VII is completely general, and could be used as the basis for the calculation of the stability of a general tokamak equilibrium to axisymmetric modes.

## ACKNOWLEDGEMENTS

This research was funded by the U.S. Department of Energy, Office of Science, Office of Fusion Energy Sciences under contract DE-SC0021156.

## DATA AVAILABILITY STATEMENT

The digital data used in the figures in this paper can be obtained from the author upon reasonable request. The TJ code is freely available at `https://github.com/rfitzp/TJ`.

---

[1] F. Troyon, R. Gruber, H. Saurenmann, S. Semenzato and S. Succi, Plasma Phys. Control. Fusion **26**, 209 (1984).

[2] R. Goldston, Plasma Phys. Control. Fusion **26**, 87 (1984).

[3] M. Huguet, K. Dietz, J.L. Hemmerich and J.R. Last, Fusion Technology **11**, 43 (1987).

[4] M. Okabayashi and G. Sheffield, Nucl. Fusion **14**, 575 (1974).

[5] K. Lackner and A.B. MacMahon, Nucl. Fusion **14**, 575 (1974).

[6] T. Pfirsch and H. Tasso, Nucl. Fusion **11**, 259 (1971).

[7] S.C. Jardin, Phys. Fluids **21**, 1851 (1978).

[8] J.A. Wesson, Nucl. Fusion **18**, 87 (1978).

[9] D. Dobrott and C.S. Chang, Nucl. Fusion **21**, 1573 (1981).

[10] D.J. Ward, S.C. Jardin and C.Z. Cheng, J. Comp. Phys. **104**, 221 (1993).

[11] R. Fitzpatrick, Phys. Plasmas **31**, 102507 (2024).

[12] R. Fitzpatrick, Phys. Plasmas **32**, 062509 (2025).

[13] J.P. Freidberg, A. Cerfon and J.P. Lee, J. Plasma Phys. **81**, 515810608 (2015).

[14] J.P. Lee, A. Cerfon, J.P. Freidberg and M. Greenwald, J. Plasma Phys. **81**, 515810607 (2015).

[15] M.N. Bussac, R. Pellat, D. Edery and J.L. Soule, Phys. Rev. Lett. **35**, 1638 (1975).

[16] J.W. Connor, S.C. Cowley, R.J. Hastie, T.C. Hender, A. Hood and T.J. Martin, Phys. Fluids **31**, 577 (1988).

[17] R. Iacono, A. Bondeson, F. Troyon and R. Gruber, Phys. Fluids B **2**, 1794 (1990).

[18] L. Guazzotto, R. Betti, J. Manickam and S. Kaye, Phys. Plasmas **11**, 604 (2004).

[19] J.P. Freidberg, *Ideal Magnetohydrodynamics*, (Plenum, New York NY, 1987).

[20] P.M. Morse and H. Feshbach, *Methods of Theoretical Physics*, (McGraw-Hill, New York, NY, 1953), p. 1301.

[21] P.M. Morse and H. Feshbach, *Methods of Theoretical Physics*, (McGraw-Hill, New York, NY, 1953), p. 1302.

[22] M. Abramowitz and I.A. Stegun, *Handbook of Mathematical Functions*, (Dover, New York NY, 1964), sect. 8.11.

[23] M. Abramowitz and I.A. Stegun, *Handbook of Mathematical Functions*, (Dover, New York NY, 1964), chap. 6.

[24] P.M. Morse and H. Feshbach, *Methods of Theoretical Physics*, (McGraw-Hill, New York, NY, 1953), pp. 1302–1309.

[25] S.W. Haney and J.P. Freidberg, Phys. Fluids B **1**, 1637 (1989).

[26] R. Fitzpatrick, Phys. Plasmas **31**, 112502 (2024).

[27] R. Fitzpatrick, R.J. Hastie, T.J. Martin and C.M. Roach, Nucl. Fusion **33**, 1533 (1993).

[28] R. Fitzpatrick, Phys. Plasmas **31**, 082505 (2024).

[29] X. Xu, Z. Chen, C. Han, L. Zhu, W. Zhang, J. Xu, C. Yang, C. Tang, N. Wang, Y. Ding, Z. Chen, Z. Yang, X. Zhang, Y. Pan and J-TEXT team, Phys. Plasmas **29**, 032510 (2022).

[30] S. Guizzo, A.O. Nelson, C. Hansen, F. Logak and C. Paz-Soldan, Plasma Phys. Control. Fusion **66**, 065018 (2024).

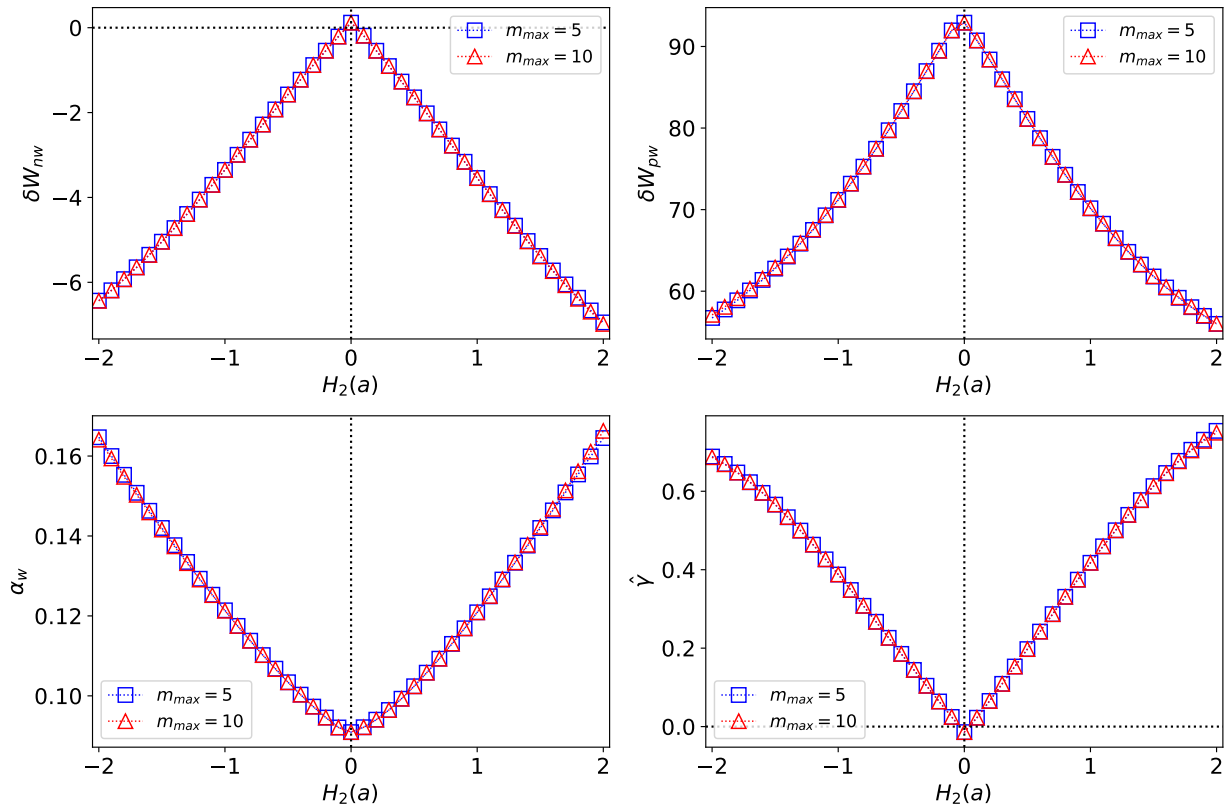


FIG. 1. The no-wall perturbed potential energy, $\delta W_{nw}$, the perfect-wall perturbed potential energy, $\delta W_{pw}$, the wall parameter, $\alpha_w$, and the normalized thin-wall growth-rate, $\hat{\gamma}$, of the unstable axisymmetric mode, plotted as a function of the plasma elongation parameter, $H_2(a)$, for plasma equilibria characterized by $\epsilon = 0.1$, $V_2(a) = H_3(a) = 0$, $q(0) = 1.01$, $q(a) = 3.6$, $p_2(0) = 0.05$, $\mu = 2.5$, and $b_w = 1.1$.

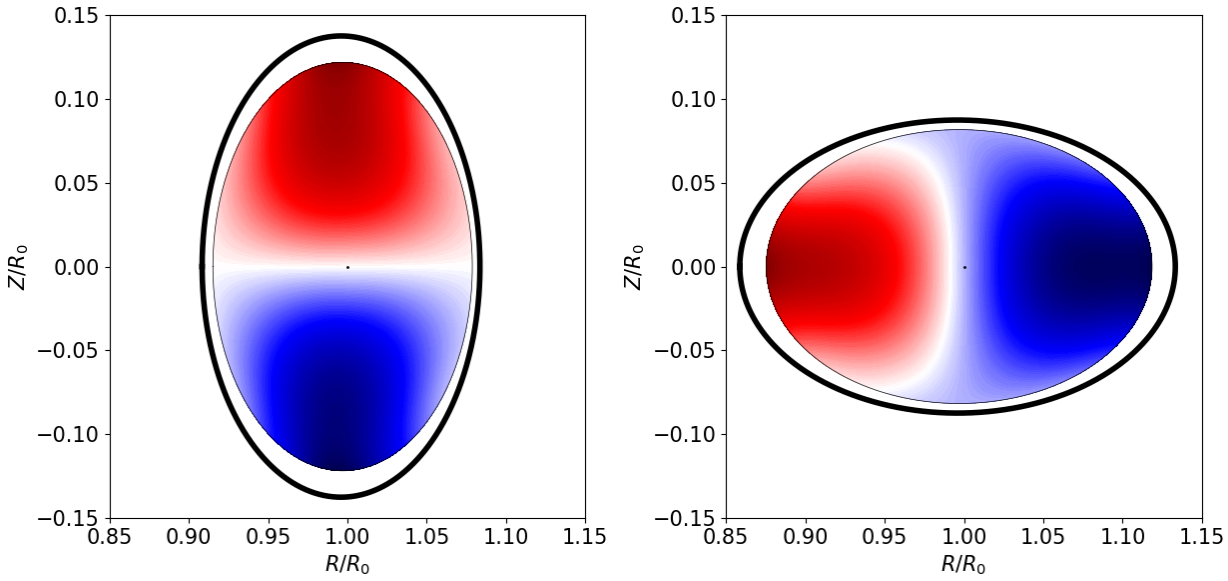


FIG. 2. The radial plasma displacement function, $y(r,\theta) = f\,\xi^r$, of the unstable axisymmetric mode for the cases $H_2(a) = +2$ (left panel) and $H_2(a) = -2$ (right-panel) that feature in Fig. 1. Here, red is positive and blue is negative. The thick black line indicates the wall.

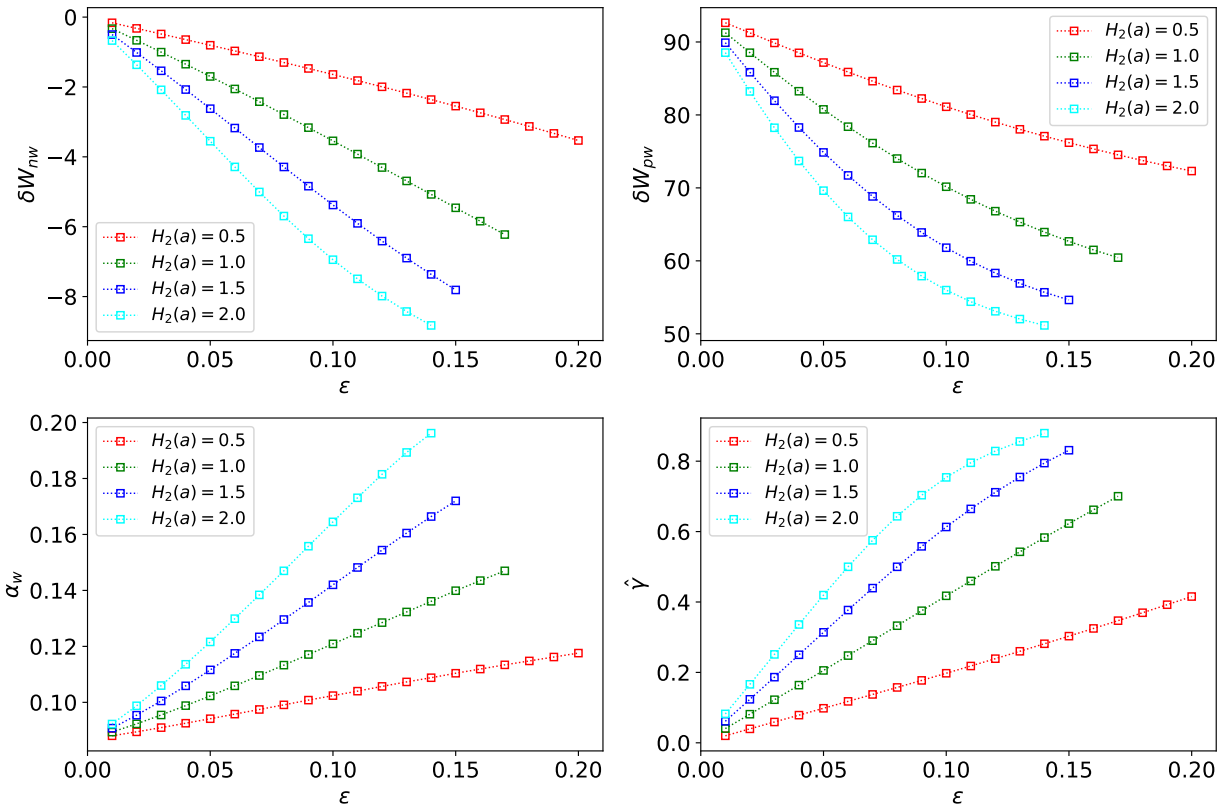


FIG. 3. The no-wall perturbed potential energy, $\delta W_{nw}$, the perfect-wall perturbed potential energy, $\delta W_{pw}$, the wall parameter, $\alpha_w$, and the normalized thin-wall growth-rate, $\hat{\gamma}$, of the unstable axisymmetric mode, plotted as a function of the plasma inverse aspect-ratio, $\epsilon$, for plasma equilibria characterized by $V_2(a) = 0$, $H_3(a) = 0$, $q(0) = 1.01$, $q(a) = 3.6$, $p_2(0) = 0.05$, $\mu = 2.5$, $b_w = 1.1$, and various different values of $H_2(a)$.

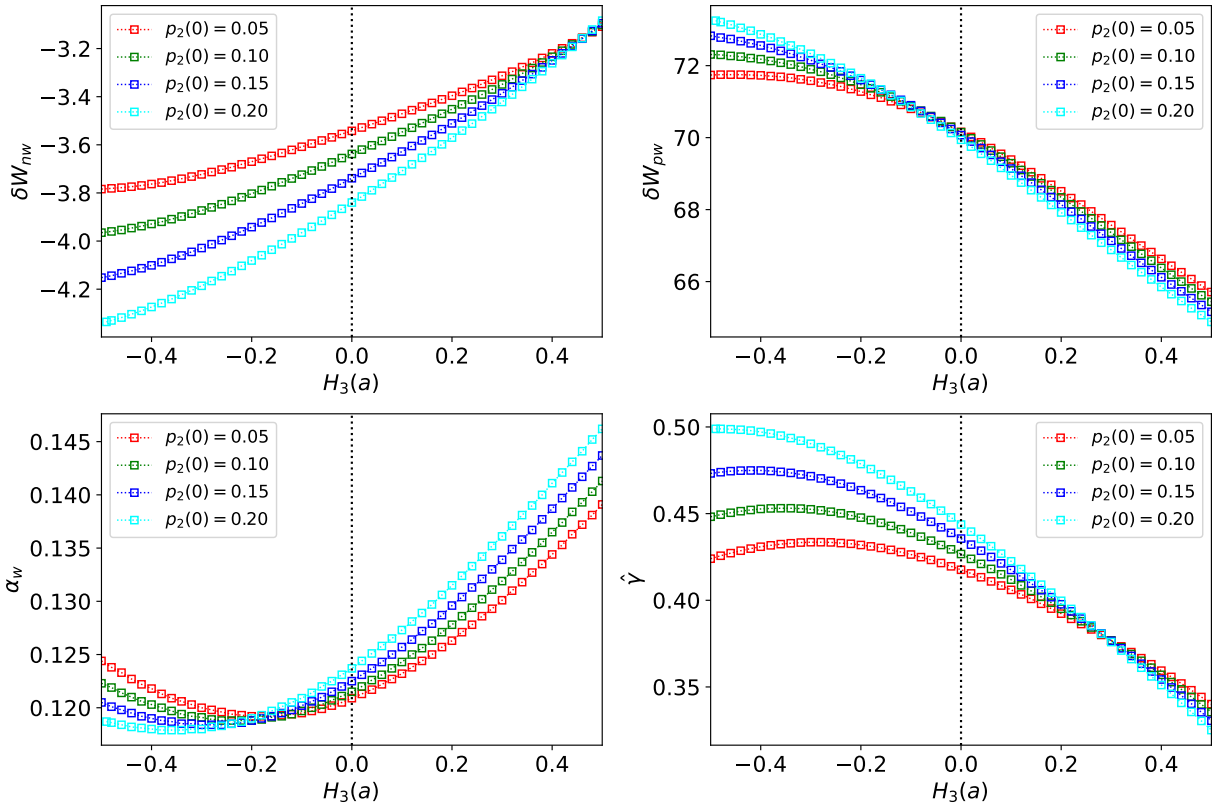


FIG. 4. The no-wall perturbed potential energy, $\delta W_{nw}$, the perfect-wall perturbed potential energy, $\delta W_{pw}$, the wall parameter, $\alpha_w$, and the normalized thin-wall growth-rate, $\hat{\gamma}$, of the unstable axisymmetric mode, plotted as a function of the plasma triangularity parameter, $H_3(a)$, for plasma equilibria characterized by $\epsilon = 0.1$, $H_2(a) = 1$, $V_2(a) = 0$, $q(0) = 1.01$, $q(a) = 3.6$, $\mu = 2.5$, $b_w = 1.1$, and various different values of $p_2(0)$.

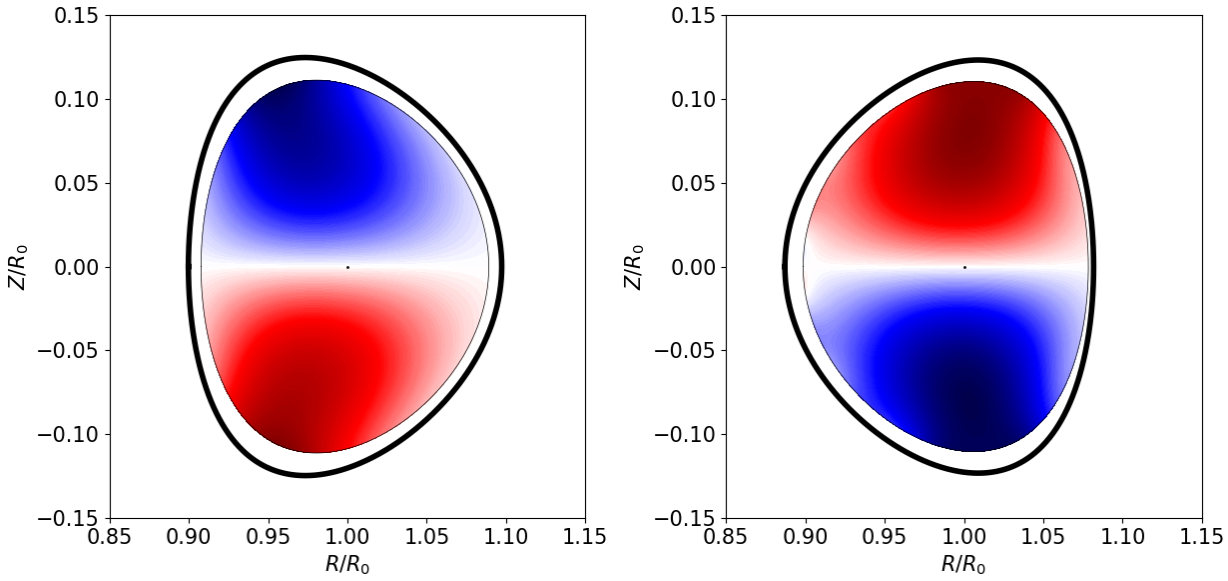


FIG. 5. The radial plasma displacement function, $y(r,\theta) = f\,\xi^r$, of the unstable axisymmetric mode for the cases $H_3(a) = +0.5$, $p_2(0) = 0.2$ (left panel) and $H_3(a) = -0.5$, $p_2(0) = 0.2$ (right-panel) that feature in Fig. 4. Here, red is positive and blue is negative. The thick black line indicates the wall.

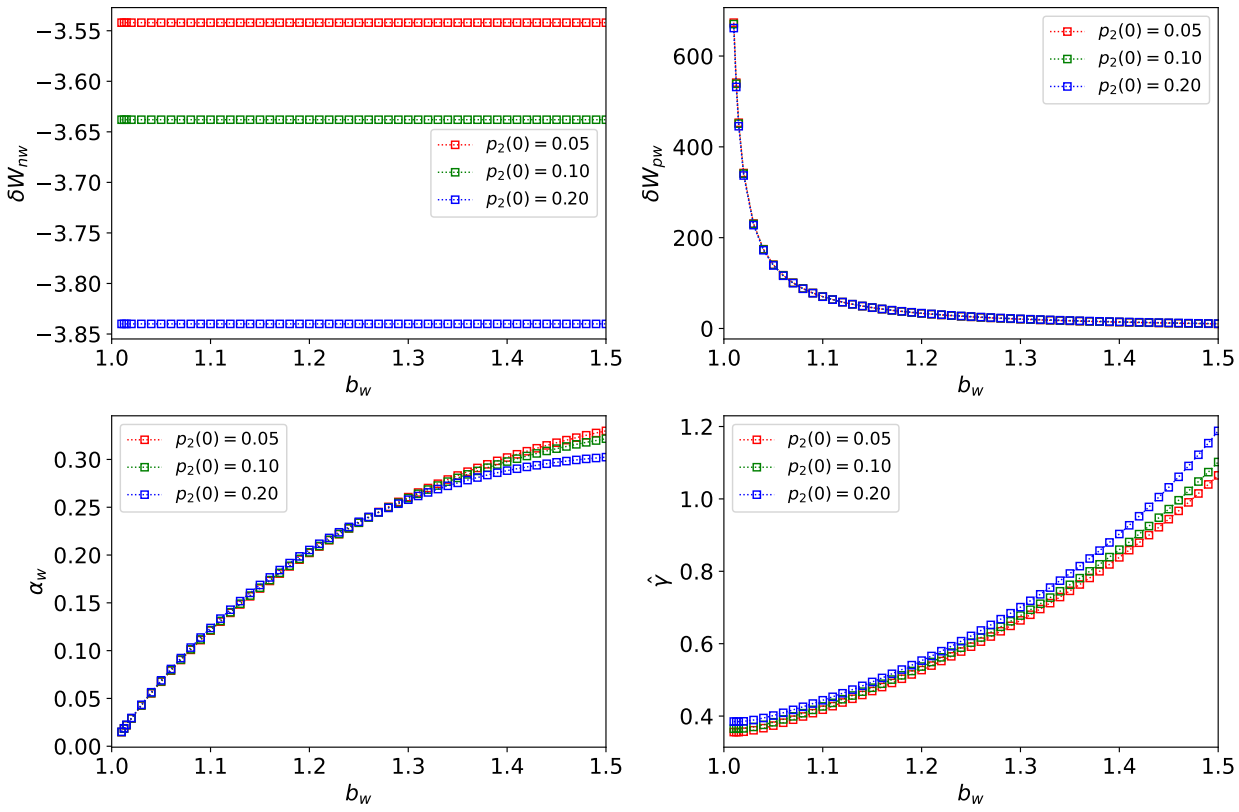


FIG. 6. The no-wall perturbed potential energy, $\delta W_{nw}$, the perfect-wall perturbed potential energy, $\delta W_{pw}$, the wall parameter, $\alpha_w$, and the normalized thin-wall growth-rate, $\hat{\gamma}$, of the unstable axisymmetric mode, plotted as a function of the relative wall radius, $b_w$, for plasma equilibria characterized by $\epsilon = 0.1$, $H_2(a) = 1$, $V_2(a) = H_3(a) = 0$, $q(0) = 1.01$, $q(a) = 3.6$, $\mu = 2.5$, and various different values of $p_2(0)$.

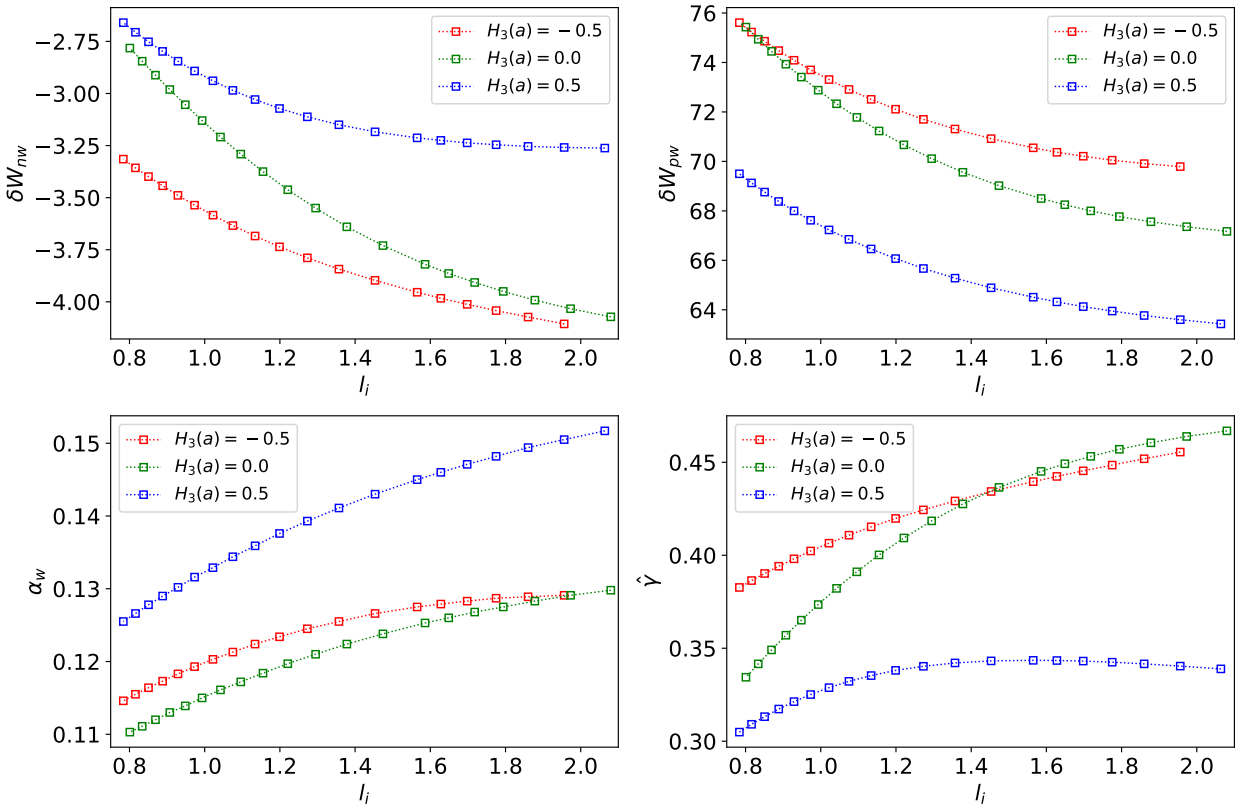


FIG. 7. The no-wall perturbed potential energy, $\delta W_{nw}$, the perfect-wall perturbed potential energy, $\delta W_{pw}$, the wall parameter, $\alpha_w$, and the normalized thin-wall growth-rate, $\hat{\gamma}$, of the unstable axisymmetric mode, plotted as a function of the plasma self-inductance, $l_i$, for plasma equilibria characterized by $\epsilon = 0.1$, $H_2(a) = 1$, $V_2(a) = 0$, $q(a) = 3.6$, $p_2 = 0.05$, $\mu = 2.5$, and various different values of $H_3(a)$.

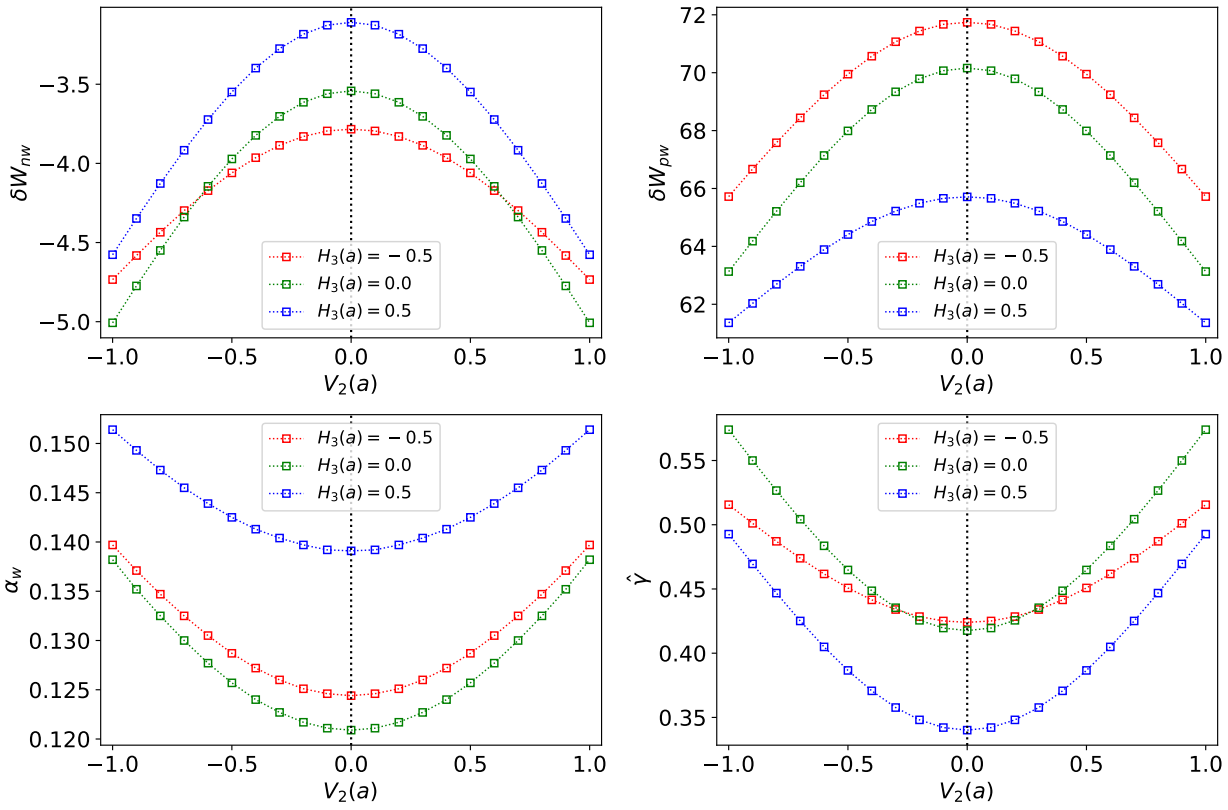


FIG. 8. The no-wall perturbed potential energy, $\delta W_{nw}$, the perfect-wall perturbed potential energy, $\delta W_{pw}$, the wall parameter, $\alpha_w$, and the normalized thin-wall growth-rate, $\hat{\gamma}$, of the unstable axisymmetric mode, plotted as a function of the plasma tilt parameter, $V_2(a)$, for plasma equilibria characterized by $\epsilon = 0.1$, $H_2(a) = 1$, $H_3(a) = 0$, $q(0) = 1.01$, $q(a) = 3.6$, $p_2 = 0.05$, $\mu = 2.5$, and various different values of $H_3(a)$.

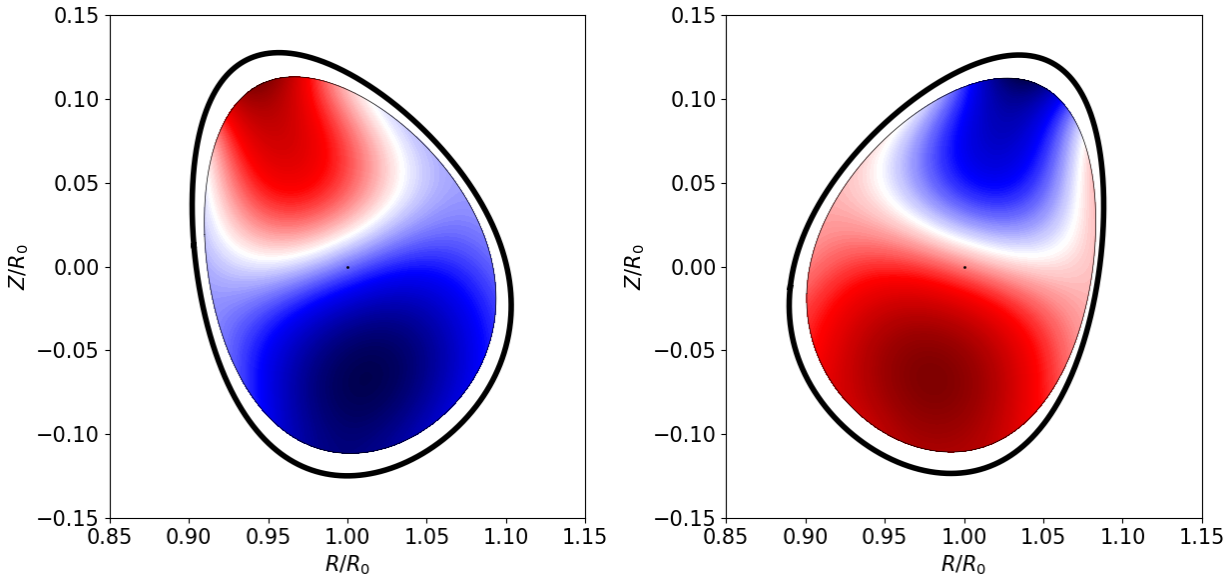


FIG. 9. The real part of the radial plasma displacement function, $y(r,\theta) = f\,\xi^r$, of the unstable axisymmetric mode for the cases $V_2(a) = -1.0$, $H_3(a) = 0.5$ (left panel) and $V_2(a) = 1.0$, $H_3(a) = -0.5$ (right-panel) that feature in Fig. 8. Here, red is positive and blue is negative. The thick black line indicates the wall.

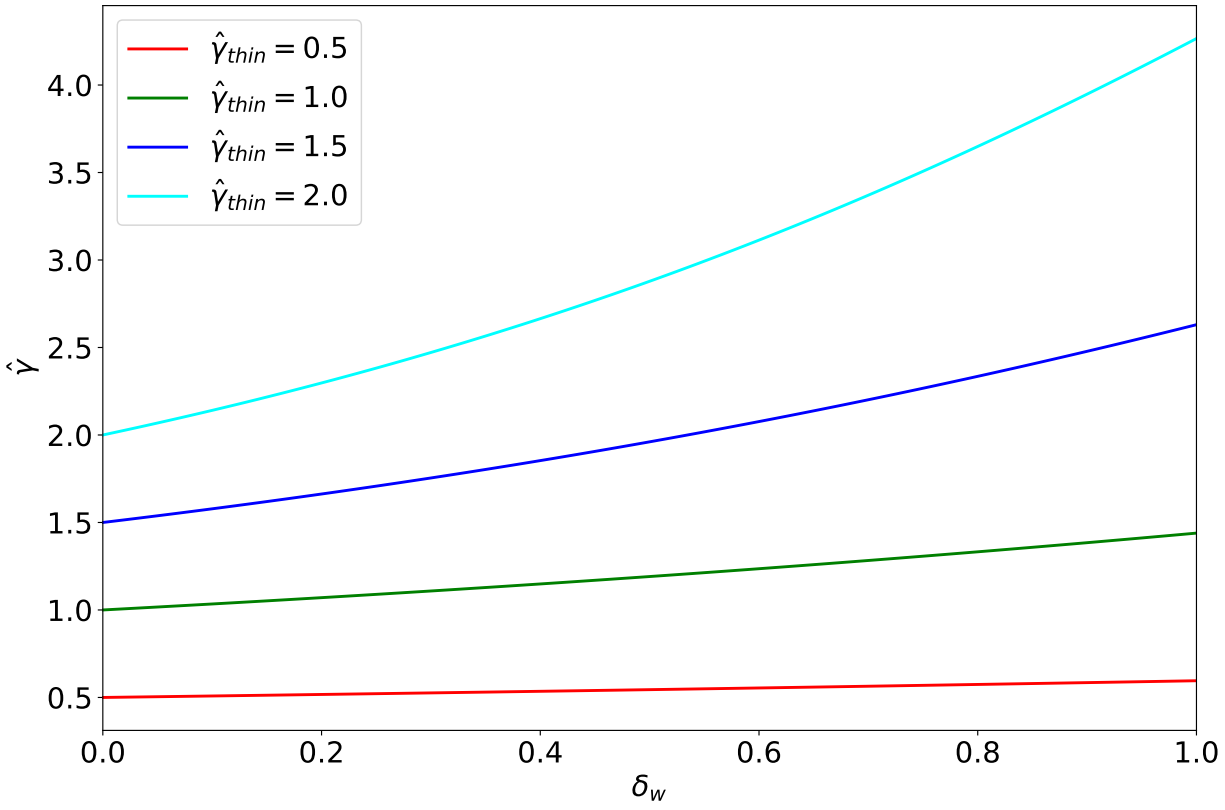


FIG. 10. Variation of the true normalized resistive wall mode growth-rate, $\hat{\gamma}$, with the wall thickness parameter, $\delta_w$, for various values of the thin-wall normalized growth-rate, $\hat{\gamma}_{\rm thin}$.